UCRL 8202

UNIVERSITY OF
CALIFORNIA

Radiation
Laboratory

POSITRON SPECTRUM FROM THE DECAY OF THE μ MESON

DISCLAIMER

UCRL-8202
Physics and Mathematics

UNIVERSITY OF CALIFORNIA
Radiation Laboratory
Berkeley, California

Contract No. W-7405-eng-48

POSITRON SPECTRUM FROM THE DECAY OF THE μ MESON

Walter F. Dudziak, Ryokichi Sagane, and James Vedder

March 20, 1958

Printed for the U. S. Atomic Energy Commission

Contents

Abstract 3
Introduction 4
Method 5
Apparatus and Procedure 6
Measurement of the Muon Mean Life 11
Measurement of the Michel Parameter ρ_M 11
Measurement of the Muon Rest Mass 31
Acknowledgments 34
Appendix
A. Ionization and Straggling: Spectrometer Resolution . . . 35
B. Effect of Saturation on the Michel ρ_M parameter 52
C. Radiation Correction 57
D. Background Determination 60

POSITRON SPECTRUM FROM THE DECAY OF THE μ MESON

Walter F. Dudziak, Ryokichi Sagane, and James Vedder
Radiation Laboratory
University of California
Berkeley, California

March 20, 1958

ABSTRACT

A magnetic spiral-orbit spectrometer was used to study the positron spectrum from an isotropic μ^+ decay. The detected positrons were identified by an electronic technique designed to measure the lifetime of the muon. Our measured weighted mean value of the μ^+ mean life is $\tau_\mu = 2.210 \pm 0.015$ μsec.

The data have been analyzed according to the simplified one-parameter theory of Michel, as modified by Behrends, Finkelstein, and Sirlin to include radiative corrections. The weighted mean value of this Michel parameter is $\rho_M = 0.734 \pm 0.022$. Also indicated is the possibility that this measured mean value could be higher by 1%. In this experiment the measurements in the low-energy positron region were not of sufficient accuracy to yield an estimate of the second Michel parameter.

Included is a measurement of the maximum positron energy. The weighted mean value of this measurement is $W = 52.87 \pm 0.07$ Mev. From this value and the simple algebraic relation to the masses of the decay particles one obtains a value of the μ^+ mass $\mu = 206.94 \pm 0.27$.

POSITRON SPECTRUM FROM THE DECAY OF THE μ MESON

Walter F. Dudziak, Ryokichi Sagane, and James Vedder

Radiation Laboratory
University of California
Berkeley, California

March 20, 1958

INTRODUCTION

Early observations of the energy of electrons from the decay of the muon have guided theoretical calculations through the many proposed assumptions for the possible mode of decay of the muon. From the experimental point of view, the most successful theoretical calculations were based on the assumption of a direct interaction between four fermions, i.e., on

$$\mu^{\pm} \rightarrow e^{\pm} + \nu_1 + \nu_2 .$$

Using this assumption for the decay scheme of the muon and the mechanics first proposed by Fermi for describing β decay, Tiomno and Wheeler[1] and Michel[2] have predicted the probable energy dependence of the $e^{\pm}$ in β decay for this process. Michel, in particular, calculated the energy distribution of the positrons from the isotropic μ-meson decay, using a linear combination of all five interactions (i.e., scalar, vector, tensor, axial vector, and pseudoscalar) for both distinguishable and indistinguishable neutrinos. In this way Michel obtained the following general expression for the energy-dependent probability of $e^{\pm}$ emission in isotropic μ-meson decay:

$$P(E)dE = \frac{(E^2 - \epsilon^2)^{\frac{1}{2}}}{3\hbar(2\pi\hbar^2c^2)^3}\,\mu\,[3E(W-E)K_1 + 2(E^2 - \epsilon^2)K_2 + 3\epsilon(W-E)K_3]dE, \quad (1)$$

where K_1, K_2, and K_3 are functions of the five Fermi coupling constants, i.e.,

$$\begin{aligned} K_1 &= g_s^2 + 2\,(g_v^2 + g_T^2 + g_A^2) + g_p^2, \\ K_2 &= g_v^2 + 2g_T^2 + g_A^2, \\ K_3 &= g_s^2 - 2g_v^2 + 2g_A^2 - g_p^2 . \end{aligned} \quad (2)$$

E and W are the total energy and maximum energy of the positron, and ε and μ are respectively the electron and muon rest mass. This transition probability can easily be rewritten in terms of two parameters that are bilinear functions of the five coupling constants:

---

[1] J. Tiomno and J. A. Wheeler, Revs. Modern Phys. 21, 144 (1949).

[2] L. Michel, Proc. Phys. Soc. A. (London) 53, 514 (1950); Thesis, University of Paris, 1953.

$$P(E)dE = \frac{1}{\tau_\mu} \frac{(E^2 - \epsilon^2)^{\frac{1}{2}}}{A + \psi B} \left[3E(W-E) + \frac{2}{3}\rho_M(4E^2 - 3EW - \epsilon^2) + 3\psi\epsilon(W-E)\right]dE, \quad (3)$$

where $\rho_M = 3K_2/(K_1+2K_2)$ and is limited to the range of values $0 \leq \rho_M \leq 1$, and $\psi = K_3/(K_1 + 2K_2)$, that is, is limited to the range of values $-1 \leq \psi \leq 1$. The terms A and B are constants that depend on the value of W. (Note: ψ = Michel's η. We reserve η so as to comform with notation in Reference 8). Thus the Michel theory predicts a family of possible energy spectra for the positrons from an isotropic positive muon decay, each of which has two free parameters that may in principle be determined experimentally. In addition to these two parameters, two other measurements can be made. These are (a) the maximum energy W and (b) the mean lifetime of the muon τ_μ. A measurement of W becomes a measurement of the muon rest mass μ because W is related to the rest masses of the interacting fermions by the expression $W = (\mu^2 + \epsilon^2)/2\mu$ when the assumption is made that the neutrino rest mass, M_ν, is 0. The purpose of this experiment was to measure these four quantities.

METHOD

We succeeded in determining three of these -- that is, in measuring τ_μ, ρ_M, and W. In what follows we deal with details of these measurements. However, a few remarks should be made about our efforts to measure the ψ parameter.

Consider the effect of ψ on the shape of the positron decay spectrum as shown by Eq. (3), (even though ψ, like ρ_M, no longer has this simple meaning when radiative corrections are considered in deriving the transition probability, Eq. (1). These corrections were ignored in the derivation of Eq. (1)). This effect of ψ on the shape of the spectrum increases as the positron energy decreases. Calculations summarized in Table I show that the difference in the ratios of the positron intensities $[P(E=10)/P(E=5)]_\psi = Q_\psi$, when evaluated at 5 Mev and 10 Mev for two ψ values at the same ρ_M value, can be as large as 10%. This is a measurable difference.

Table I

Ratios of $Q = \frac{P(E=10)}{P(E=5)}$ for different ψ values

ρ_M	Calculated ratio for value of Q at $\psi = -1$ to value at $\psi = 0$	Calculated ratio for value of Q at $\psi = 0$ to value at $\psi = +1$
0.50	1.088	1.070
0.70	1.115	1.086
0.75	1.146	1.092

In our experiment we obtained the ratios from the intensity measurements at three positron energies in this low-energy region. The lowest positron energy at which measurements were made was 5 Mev. In the

reduction of these data we found that the background contribution to the measured intensity was comparable to the contribution arising from positrons leaving the target. For this reason, and because there is some ambiguity in determining the magnitude of this background in the very-low-energy region (Appendix D), we feel that these intensity measurements are not reliable. Therefore they are omitted in the presentation of our data and no estimate is made of the value of the ψ parameter.

The measurements of τ_M, ρ_M, and W are related to the same general experimental procedure. Except for target modifications and other parameters that affect the resolution of a measurement, the experimental procedure was the same. We discuss it here in a general way and present the details in the appendixes.

APPARATUS AND PROCEDURE

Measurements were made by using a spiral-orbit spectrometer[3] for determining the momentum distribution and a quadruple-coincidence electronic technique for identification of positrons from a muon decay.

Figures 1, 2, and 3 are very useful for the understanding of our experiment. They represent schematically the general features of our procedure. As shown in Fig. 1, a pulsed proton beam was introduced along the magnetic axis of a spiral-orbit spectrometer. It was used to create pions in a lithium target that was mounted coaxially with the magnetic axis. Those pions that were created with insufficient energy to emerge from the target decayed inside the target into muons that in turn disintegrated, giving birth to positrons. The energy spectrum from this positron source was magnetically analyzed by means of the spiral-orbit principle, as shown in Fig. 2.

The positrons were detected as quadruple coincidences of signals from four plastic scintillators (three were 3 by 3 by $\frac{1}{4}$ in., and the fourth one 4 by 4 by $\frac{1}{2}$ in.) As illustrated in Fig. 3, counts were taken between proton pulses during four consecutive gates each having a 2-microsecond width. The start of the first gate was delayed by 3 μsec relative to a proton pulse. The full width of each proton pulse was < 0.5 μsec. This counting procedure enabled us to use the same counts as determined the shape of the electron spectrum from the muon decay for a measure of τ_μ (that is,

---

[3a] G. Miyamoto, Proc. Phys.-Math. Soc. Japan (in Japanese) 17 557 (1943)

[3b] Iwata, Miyamoto, and Kotani, J. Phys. Soc, Japan 2, 1 (1947) (in Japanese; English translation by Ryokichi Sagane, UCRL translation 111).

[3c] Sagane, Miyamoto, Nakamura, and Takechi, Proc. Phys.-Math. Soc. Japan 25, 274 (1943).

[3d] M. Sakai, J. Phys. Soc. Japan 5, 178 (1950); J. Phys. radium 14, 570 (1953).

[3e] Walter Dudziak, Production Cross Sections for Positive and Negative Pions from Carbon Initiated by 340-Mev Protons (thesis) UCRL-3564) Apr. 1954.

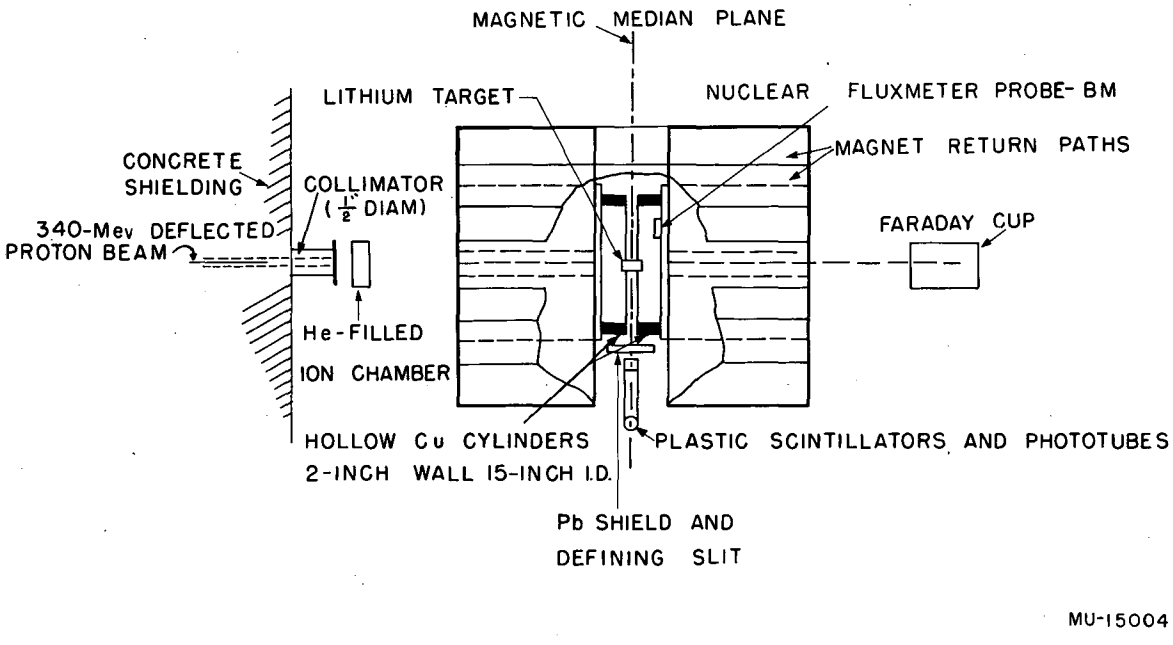

Fig. 1. Schematic diagram of the experimental arrangement.

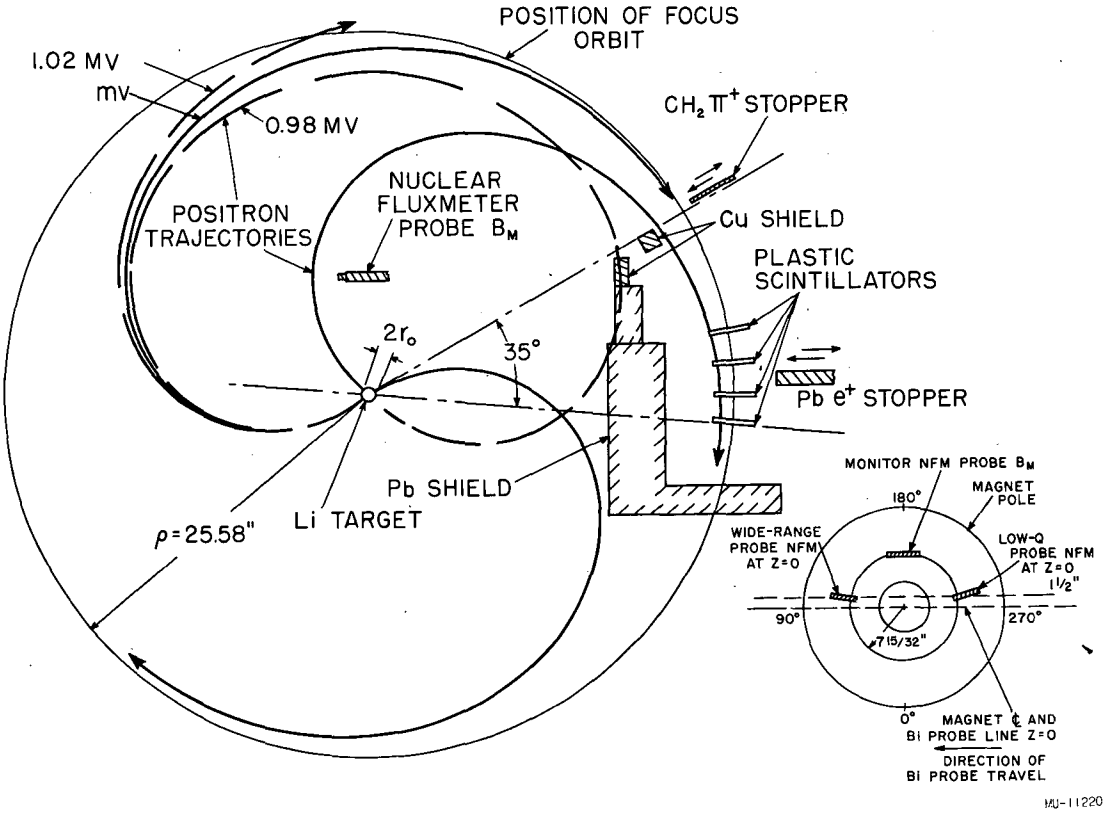

Fig. 2. (left) Section at the median plane of the spectrometer for the muon experimental geometry

(right, below) Schematic diagram of experimental arrangement used to measure the radial magnetic-field distribution.

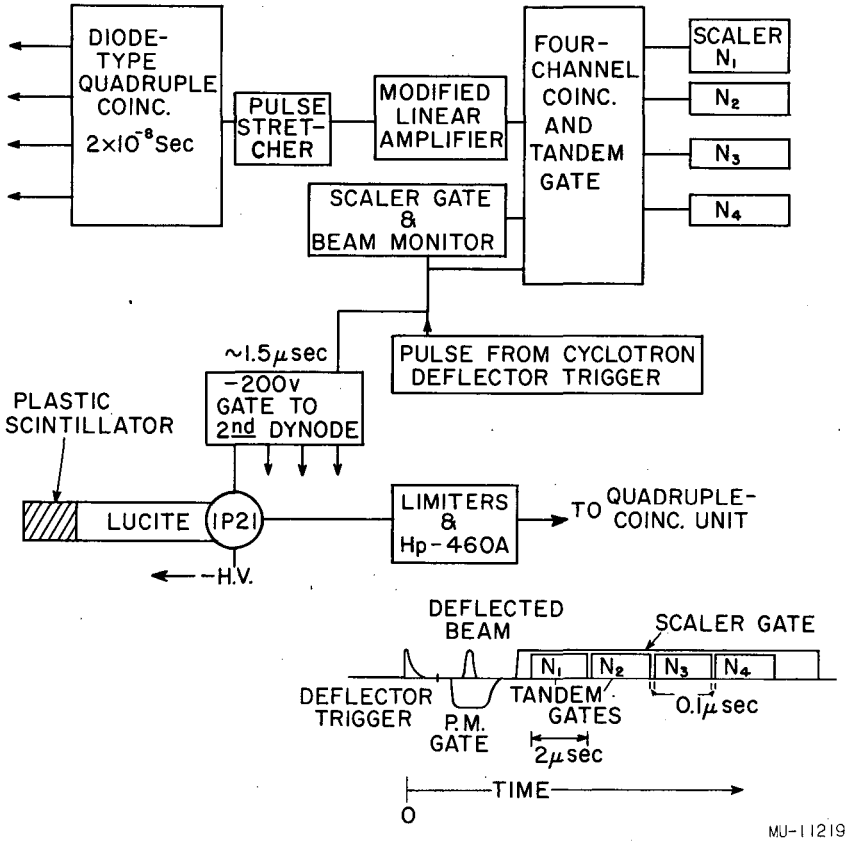

Fig. 3. Block diagram of the electronic gates and timing system.

the mean life of the muon). The 3-μsec delay after a proton pulse was sufficient to decrease to < 2% the accidental background at our highest counting rate and largest possible proton pulse. This background is defined as the count measured by introducing a 1-inch lead positron stopper between Scintillators 2 and 3. During the course of the experiment the magnitude of an average proton pulse was $\leq \frac{1}{2}$ the pulse responsible for this background.

During earlier experiments we found that the count from our first gate consistently fell below the straight-line plot determining the mean life of the muon. This was caused by insufficient recovery time for the slow electronics following a voltage overload brought about by secondaries produced during the proton pulse. Depending on the size of the proton pulse, such recovery time can be as large as 15 μsec. To eliminate this problem we used

(a) a negative voltage pulse applied to the second dynode of each photomultiplier during the time of the proton pulse (illustrated in Fig. 3),

(b) a series of pulse-height limiters,

(c) a modified slow amplifier giving a moderately fast recovery -- that is, from 2 to 2.5 μsec after a maximum proton pulse overload that occurred in the absence of (a) and (b).

Effects of temperature variations on all electronic components were studied. Components that could not withstand the day-to-day temperature variations without drifting were enclosed in a temperature-controlled atmosphere held constant to within 1°C. These precautions eliminated drifts and permitted even day-to-day reproducibility of the standard check points we adopted. In addition, a continuous check on the reliability of the tandem gate circuit was obtained by splitting the pulse from the modified linear amplifier, and passing one part of it through a variable gate and then through a second tandem gate unit. (This is not shown in Fig. 3.) A variable gate has the property of converting any pulse above a preset pulse height into a constant-output voltage pulse that has a fixed shape. Other standard electronic tests were made on variations that could introduce systematic errors into our results. These included measurements of

(a) counting-rate uniformity across the surface of each scintillator,

(b) high-voltage plateaus on each photomultiplier,

(c) effect of magnetic-field variation on photomultipliers in magnetic shields. (This test covered twice the magnetic-field variations that occurred during the experiment),

(d) cable-length plateaus of the fast-electronics system, and

(e) proton-monitor plateaus.

We found that under certain proton beam conditions argon-filled ion chambers[4] gave false indications of the true number of protons. We

[4] Segrè-Wiegand type; see Reference 3e.

attribute this to recombination in the highly ionized regions of the gas resulting from the passage of an intense proton pulse. For this reason we used a modified helium-ion chamber in tandem with a Faraday cup. This permitted a continuous check of our proton monitor, which was found accurate for variations of a factor of nine in the proton-beam intensity. No such variations of the proton beam intensity were allowed to occur during the course of our experiment.

MEASUREMENT OF THE MUON MEAN LIFE

The data presented in this paper as a measure of the Michel parameter were obtained during twelve different days. For each day the counts obtained during each gate were also added together. From this sum the accidental background for that gate was subtracted and then divided by the proper time width of the gate. By means of the method of least squares[5] we fitted a straight line to the semilog plot of the results from the four gates, and obtained the most probably value for the slope of the linear equation that determines the mean life of the muon, τ_μ. We also calculated the standard deviations of the constants defining the linear form of the equation. The mean life obtained from these calculations is displayed in Column 2 of Table II as the mean life measured by the counts for that particular day. Column 3 of Table II represents the corresponding standard deviation obtained from a statistical treatment of the data for that day. Basing the weights on the statistial errors as given in Column 3, one obtains $\tau_\mu = 2.210 \pm 0.015$ μsec for the weighted mean value of the positive muon mean life. (See Appendix E for calibration of time scale.)

MEASUREMENT OF THE MICHEL PARAMETER ρ_M

A value of the Michel ρ_M parameter can be determined (a) from a measure of a ratio of the counting rates at two positron energies near the high-energy end of the spectrum,[6] or (b) from the measured shape of the positron decay spectrum. Both these methods were used. As will be shown, the first of these methods is inferior to the second because of the greater influence of possible unknown systematic errors on the measurement of this Michel parameter. For each of these methods a momentum-analyzed positron beam arising from the decay of the muon is necessary. The momentum analysis was obtained by a new type of magnetic spectrometer that permits large solid-angle focusing with good resolution (Appendix A). This spectrometer property arises from a nonuniform radial magnetic field (as shown in Fig. 4) that is symmetric about the magnetic axis (and therefore also about the axis of a cylindrical source that is placed coincident with it). The position of the focus orbit is determined by the shape of the magnetic-field distribution. This shape must remain unchanged if

---

[5] Raymond T. Birge, Phys. Rev. 40, 207 (1932); Am. J. Phys. 7, 351 (1939).

[6] Sagane, Dudziak, and Vedder, Bull. Am. Phys. Soc. 4, 174 (1956).

the focus-orbit position is to remain unchanged when the magnitude of the magnetic field is varied. Furthermore, in this spectrometer the resolution is very sensitive to very small changes in the shape of the magnetic field near the focus orbit. With the aid of improved magnetic measuring techniques (see Fig. 2), permitting a continuous display of radial position and the corresponding magnetic field at that radial position, we have found that there were small variations in field shape during our earlier measurements of the high-energy region of the μ-meson decay spectrum (Appendix B). The most significant measurements that determine the Michel ρ_M parameter are in this high-energy region. Hence a large systematic error was introduced by these variations into the preliminary report of our early measurements.[7] From extensive experimental tests, which included a study of the corrections necessary for the previously reported measurements, we conclude that these difficulties were corrected by our reshaping of the magnetic field (Appendix B) and therefore did not affect the subsequent measurements.

Table II

Measurement of the mean life of the μ meson

Trial	τ_μ (μsec)	σ_{τ_μ} (μsec)
1	2.208	0.022
2	2.277	0.045
3	2.220	0.086
4	2.224	0.075
5	2.224	0.041
6	2.216	0.047
7	2.168	0.108
8	2.184	0.072
9	2.168	0.080
10	2.175	0.065
11	2.146	0.081
12	2.159	0.070

Weighted mean value = $\overline{\tau}_\mu$ = 2.210 ± 0.015 μsec

As shown in Fig. 2, the magnitude of the magnetic field was established by the frequency setting of a nuclear fluxmeter that was located in the flat region of the magnetic-field distribution. By calibration, each frequency setting was related to the vector potential at the focus orbit. We define E'_o as the total positron energy that is obtained from this vector potential. During each intensity measurement the magnetic field at the position of the nuclear fluxmeter was continuously monitored. Our magnet-current regulation was such that a drift of only ± 1 gauss in 7,000 gauss was observed during this measurement. From this and the calibration methods that were used (Fig. 2) we estimate that the accuracy of the absolute value

[7] Sagane, Dudziak, and Vedder, Phys. Rev. 95, 863 (1954).

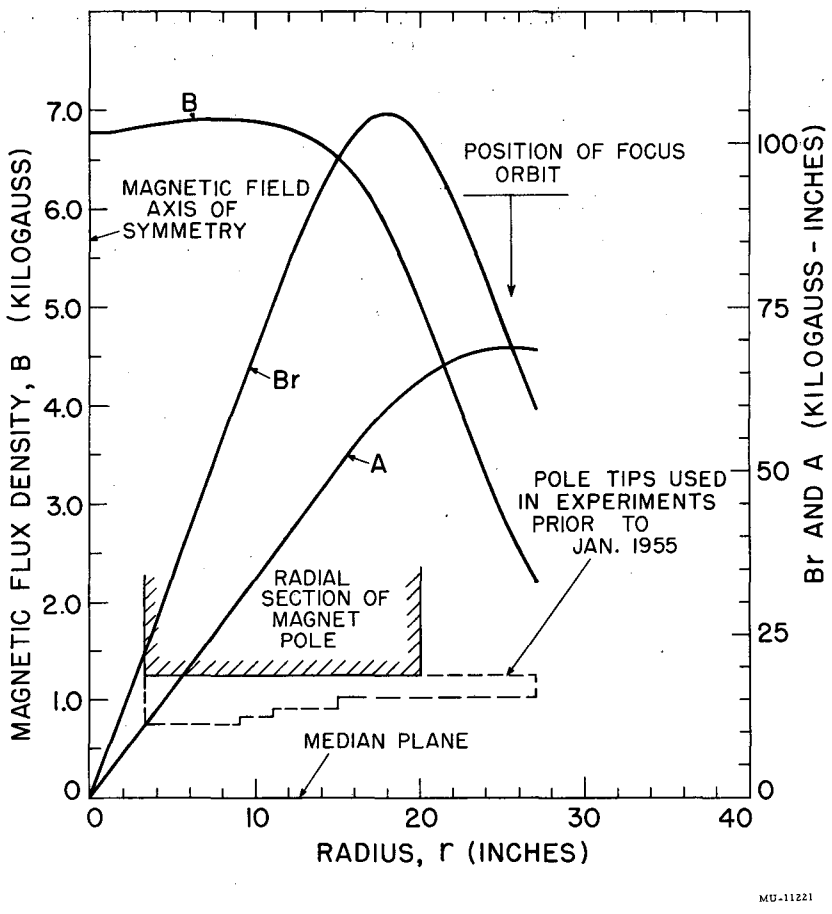

Fig. 4. Radial plot at one energy setting of the measured magnetic-field density and calculated vector potential in the median plane of the spectrometer.

of each E_0' setting is better than 0.2%.

In order to compare the Michel theory with experiment and determine the proper Michel parameter ρ_M, we must first modify Eq. (3) to incorporate the radiative corrections that have been omitted from the original derivation. It has been shown[8] that if one neglects the mass of the electron (ϵ=0) in Eq. (3) and introduces these radiative corrections into the theory one obtains the following expression for the probably energy distribution of positrons resulting from an isotropic positive muon decay:

$$\{P(\eta)\}\, d\eta = \frac{4}{\tau_\mu}\ \eta^2 \left[1 + h(\eta, \Delta E) - \Lambda_1(\Delta E)\right] \left[3(1-\eta) + \frac{2}{3}\rho_R \left\{4\eta - 3 + \Lambda_1(\Delta E)\,\eta - 3\,\Lambda_2(\Delta E)(1-\eta)\right\}\right] d\eta, \tag{4}$$

where ρ_R is related to the Michel parameter ρ_M by

$$\rho_R = \frac{\rho_M}{\left[1 + \Lambda_1(\Delta E) - \frac{2}{3}\rho_M \left\{\Lambda_1(\Delta E) - \Lambda_2(\Delta E)\right\}\right]} \tag{5}$$

Here $\eta = E/W$, W is the maximum positron energy, and ΔE is the acceptance-energy interval that is used in the experiment. The expression for $h(\eta, \Delta E)$ depends on the type of interaction that occurs between the particles during the disintegration process. For our calculations we have chosen the expression for vector coupling, which -- to the accuracy of the calculations as given by Behrends et al.[8] -- is also the expression for axial vector coupling. This expression is presented in Appendix C along with tabulated results for different values of ΔE. Found also in this appendix are the defining expressions and numerical results of the integral functions $\Lambda_1(\Delta E)$ and $\Lambda_2(\Delta E)$. Since their values depend on the function $h(\eta, \Delta E)$ they also depend on the assumed coupling describing the nature of the interaction.

As shown by the tabulated results, $h(\eta, \Delta E)$ and, to a lesser extent, $\Lambda_1(\Delta E)$ and $\Lambda_2(\Delta E)$ are varying functions of the energy interval ΔE that is used in the experiment. This ΔE energy dependence of $h(\eta, \Delta E)$ increases with positron energy. In addition, the resolution of a detecting system can be only crudely approximated by a rectangular resolution of energy width ΔE for one specific positron energy. The ΔE width of this approximation is not constant in an experiment, (but varies with the positron energy as illustrated by the well-known magnetic spectrometer behavior that $\Delta P/P$ (or in this case $\Delta E/E$) is equal to a constant. In addition, because electrons lose energy by ionization and radiation prior to leaving the target, the resolution of the combined system no longer possesses this simple spectrometer property. Proper account must be taken of this energy dependence (i.e.,

[8] Behrends, Finkelstein, and Sirlin, Phys. Rev. 101, 866 (1956).

of the variable resolution width), since this ΔE dependence of $h(\eta, \Delta E)$ will affect the shape of the spectrum near the end point, and since the Michel ρ_M parameter that describes the shape of the spectrum is primarily determined by measurements near the end point.

Our procedure for determining the proper theoretical curves to be used for comparison with our measurements follows. Figures 18 through 21 in Appendix A illustrate some of our resolution functions. Each resolution function was subdivided into varying ΔE increments that correspond to the ΔE increments of the tabulated $h(\eta, \Delta E)$ functions. At a specific positron energy η the weight of each ΔE increment is given by $\omega(\Delta E, \eta)$ where

$$\int_0^{\Delta E \text{ max}} \omega(\Delta E, \eta)\, d(\Delta E) = 1.$$

We define the weighted functions $h(\eta, \overline{\Delta E})$, $\Lambda_1(\eta, \overline{\Delta E})$, and $\Lambda_2(\eta, \overline{\Delta E})$ at a particular positron energy η by

$$f(\eta, \overline{\Delta E}) = \int_0^{\Delta E \text{ max}} f(\Delta E, \eta)\, \omega(\Delta E, \eta)\, d(\Delta E), \qquad (6)$$

where $f(\eta, \Delta E)$ symbolizes one of these functions. These weighted functions were calculated for each η value. For each chosen Michel ρ_M parameter we used the weighted functions $\Lambda_1(\eta, \Delta E)$ and $\Lambda_2(\eta, \Delta E)$ to determine $\rho_R(\eta, \overline{\Delta E})$ for each positron energy η from Eq. (5). These weighted functions, $\rho_R(\eta, \overline{\Delta E})$ and $h(\eta, \overline{\Delta E})$, were then substituted into Eq. (4) to determine the proper value of the probability function $\{P(\eta)\}_{\rho_M}$ at each η value. In our calculations we used $\Delta\eta = 0.01$ as our mesh. Following this procedure we constructed the proper family of theoretical curves for ρ_M (0.65 to 0.80), with ρ_M varying by 0.01 that are applicable to the reduction of our experimental data. In what follows we refer to these curves as modified Michel curves.

For each geometry and each ρ_M value the expected measured intensity was obtained by folding the calculated resolution curve (Appendix A) that was obtained at each E_0' value into each one of this family of modified Michel curves. The term E_0' represents that positron energy that is obtained from a measure of the vector potential at the focus orbit. For these folding numerical calculations an 0.08-Mev "mesh" was used (i.e., the interval between calculation values was 0.08 Mev.) In this way a table of expected theoretical intensities versus values of ρ_M was calculated at each measured E_0' energy for each geometry of our spectrometer.

Figures 5 and 6 summarize the raw experimental data obtained in our measurements of the Michel ρ_M parameter by the two different methods. These were the data used in Table II to yield a measure of the mean life of the muon. (By "raw data" at an E_0' energy we mean actual counts minus accidental background -- previously defined and very small -- per unit proton monitor, divided by the magnetic field that corresponds to the

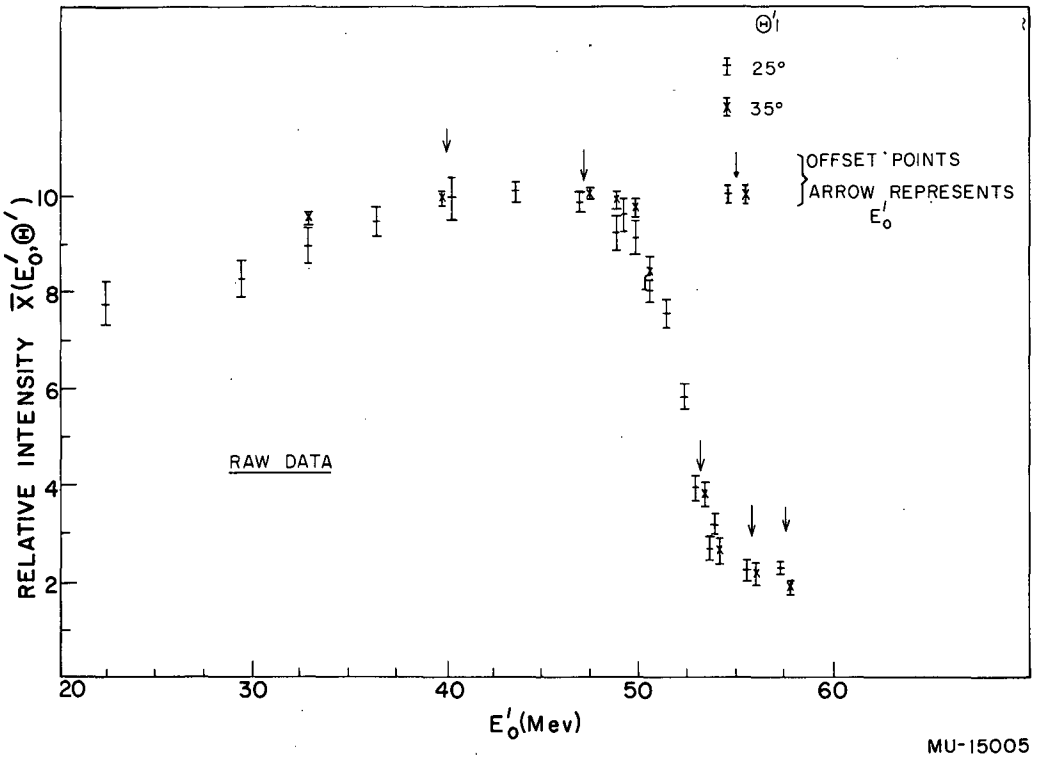

Fig. 5. Actual measured intensities as obtained for two spectrometer geometries with a solid 1-inch-diameter lithium target.

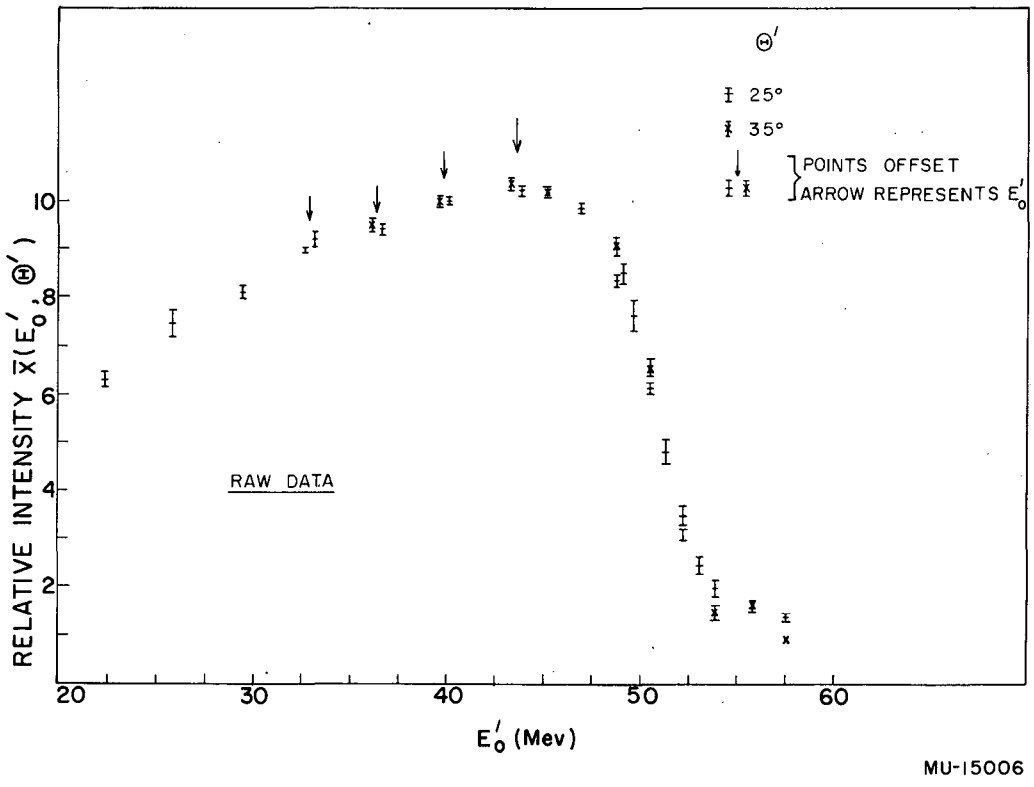

Fig. 6. Actual measured intensities as obtained for two spectrometer geometries with a solid 2-3/8-inch lithium target.

frequency setting of E_0' by a nuclear fluxmeter.) The plotted errors are standard deviations as obtained by the rule of propagation of errors.

As shown by these figures, our data for measuring ρ_M from the shape of the spectrum were obtained with four variations of the spectrometer resolution -- two of these were changes in target diameter and two of these were changes in the "angular slit" Θ' defined by the detector (see Appendix A). Data for determining ρ_M by the ratio method were obtained by two variations of the spectrometer resolution. It was measured with one "angular slit" ($\Theta' = 25^\circ$) and with lithium targets of two different diameters (2-3/8 inch and 1 inch). Each point was obtained by combining the data from a series of measurements at each E_0' energy arising from frequent repeated changes of the magnetic field that covered the listed E_0' values for each spectrometer geometry. In the ratio method as many as forty resettings and remeasurements were made at one energy.

All our data are in accordance with Chauvenet's criterion for maximum acceptable deviations that occur in repeated measurements. A very small amount of our data ($\lesssim 1\%$) was thrown out by this criterion. This amount is insignificant and would not influence the plotted data.

The data from each of the two tandem gates were analyzed and compared for possible systematic error resulting from the use of these gates. The two sets of data were in very good agreement (easily within the indicated statistics in these figures). Since these two sets of data are not independent, only one set of these results is used (actually the arithmetic mean is used).

As previously stated, a pulsed 340-Mev proton beam was incident along the axis of magnetic symmetry upon the target. Only those pions (which are created by nuclear interaction of these protons with the target) whose energy was insufficient for them to escape from the target decayed into muons which in turn yielded positrons. All other pions, which escaped from the target and impinged on areas that could not be properly screened from the detector without destroying the experimental geometry, became a source of serious positron background. One is handicapped, in an experiment measuring the Michel ρ_M parameter, by this positron background that originates from the same decay scheme as the desired positron source, because electronic techniques that measure lifetime cannot be used to discriminate against it. Since no intense pion beams were available at the time of this and another spectrometer experiment[9] one had no choice but to tolerate and allow for this background.

One cannot truly measure the total contribution from this background to the raw experimental data with the geometry as it is used during the actual experiment. Some indirect means are used to established part of the total contribution to this background. It is here where the true value of the measured Michel ρ_M parameter can be lost. That a complete understanding of this background in the present existing spectrometer experiments is

[9] Crowe, Helm, and Tautfest, Phys. Rev. 99, 872 (1955); also new experiment (unpublished).

imperative to a true prediction of the measured ρ_M parameter is illustrated in Fig. 7 by the data from one of the four geometries used in our experiment.

In Fig. 7 we replot the raw data shown in Fig. 6, which were measured with the $\Theta = 35^\circ$ geometry. In addition we present experimental measurements above $E_0' = 57.5$ Mev that are not included in Fig. 6. The point on this plot shown at $E_0' = 57.5$ Mev is a very accurate measurement. At this magnetic setting our counting rate from the desired positron source (i.e., the lithium target) should be zero, because at this E_0' energy there is no overlap of the two curves in the fold of the modified Michel curve and the resolution curve for this geometry (Fig. 20, Appendix A). Shown also on this plot are four background curves. One of these curves, indicated by b_0, is the background for this geometry as established by the methods described in Appendix D. The other three curves indicated by b_i ($i \neq 0$) are assumed background curves that are used to stress the influence of this background on the measured ρ_M parameter. Because of their importance we tabulate the results on Fig. 7 giving the value of the Michel ρ_M parameter that is obtained from a χ^2 test of the data resulting from subtraction of the chosen background from the raw data.

Realizing the seriousness of a wrong estimate of this background, we have assumed as much as 50% more error in our established background in the lower-energy region prior to the reduction of our most accurate measurements (Fig. 6). (For this reason we feel that we are conservative in our reporting of the accuracy of our experimental data by the errors as shown in Figs. 8 and 10. That this is probably true for at least the data in Fig. 8 is illustrated by the meaning of the results of our χ^2 test.)

The χ^2 test is a very suitable statistical method for determining what member of the Michel family of curves agrees best with the measurements. As seen in Eq. (3), we are confronted with the problem of determining a particular Michel distribution that contains two unknown parameters (ψ and ρ_M) about whose values we possess only such information as may be derived from the set of our observations. We may simplify our problem to that of determining only the unknown parameter ρ_M under one of the following conditions:

(a) when the parameter ψ is very close to 0 (it is zero in the two-component theory);

(b) for $\psi = \pm 1$, when the accuracy to which the parameter ρ_M is to be determined by the high-energy end of the spectrum is not in the neighborhood of 1 or 2%. (If there is a parameter $\psi = \pm 1$, neglecting it in the calculations that determine ρ_M would contribute an error in ρ_M of approximately 0.01. Whether or not this error is larger depends on the high-energy points considered. A positive value of the parameter ψ would raise the ρ_M value by this amount, whereas a negative value would lower it.) In our reduction we use the simplification (a) and determine the proper Michel curve by solving for the one unknown parameter ρ_M by the χ^2-minimum method of estimation. The requirement of this method is to find the most likely ρ_M parameter so as to render the expression

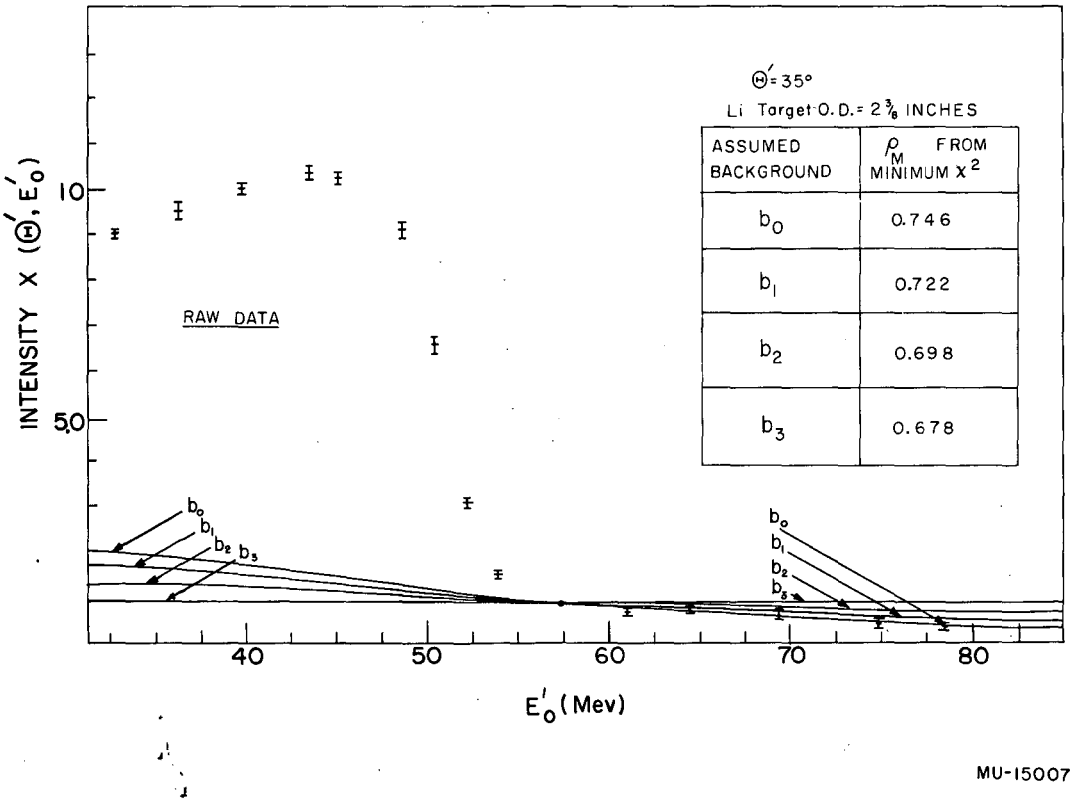

Fig. 7. Illustration of the serious effect on the Michel parameter of the subtracted background that arises from decaying muons in regions others than the desirable spectrometer source.

$$\chi^2 = \sum_{E_0'} \sigma^{-2}(E_0') \left[I(E_0') - P(E_0', \rho_M) \right]^2 \qquad (7)$$

a minimum. We limit the sum to only those E_0' values whose measured intensities are greater than 2 on the ordinate scale of the reduced data (Figs. 8, 10, etc.), so as to avoid measurements that are greatly influenced by the magnitude of the subtracted background. In this equation $I(E_0')$ is the experimental intensity measurement at an E_0' setting, $\sigma(E_0')$ is the standard deviation of this measurement, and $P(E_0', \rho_M)$ is the corresponding theoretical intensity for a specific ρ_M value. We have previously shown how for each experimental geometry a table of expected intensities $P(E_0', \rho_M)$ versus ρ_M was determined for each E_0' setting from the Michel family of curves, by calculations involving the fold of the function expressed by Eq. (4) and the function expressing the resolution at a specific E_0' setting.

Because of the experimental errors in the measured $I(E_0')$ intensities, some care is necessary in locating the proper normalization factor that fixes the ordinate scale of $I(E_0')$ in relation to the $P(E_0', \rho_M)$ scale before Eq. (7) can be used correctly in evaluating the χ^2 for a specific ρ_M value. In only a few of the many calculations presented in this paper was it found that normalization by area of the experimental measurements and the predicted measurements was correct. The proper normalization factor in our use of Eq. (7) was found by (IBM-650) calculations which were initiated by using an area normalization. This resulting χ^2 value was then compared with a newly evaluated χ^2 value based on a normalization factor that was slightly larger or smaller than the area normalization factor. By repetition of this hunting process a minimum χ^2 was determined at each ρ_M value. It is this minimum χ^2 that is plotted at each ρ_M value in Figs. 8, 10, 11, and 12. We stress this point on normalization because, from our experience -- even with as fine a ρ_M mesh ($\Delta\rho_M = 0.01$) as is used in our calculations--a difference of 0.01 to 0.015 would have been introduced into the reported ρ_M value as determined by the minimum χ^2 method by using only area normalization. (Our ρ_M value would have been lower.)

Presented in Fig. 8 are the data that were shown in Figs. 6 and 7 for the $\Theta' = 35^\circ$ geometry from which the background (as determined by methods discussed in Appendix D) has been removed. Shown also are the expected $P(E_0', \rho_M)$ values for $\rho_M = 0.65$, 0.70, and 0.75 that have been normalized by the minimum-χ^2 method as discussed above. For convenience the calculated $P(E_0', \rho_M)$ values at each ρ_M are connected by a continuous curve. Except at the measured E_0' values these curves are not to be interpreted as obtained from IBM calculations. Also plotted in this figure are the calculated results as obtained from Eq. (7). For convenience these results are likewise connected by a smooth curve.

We determine the best value of ρ_M from the minimum χ^2 of the plotted χ^2 calculations. This minimum is determined by setting equal to zero the first derivative with respect to ρ_M of a parabolic equation that is first obtained from a least-squares fit of the plotted χ^2 values. This best

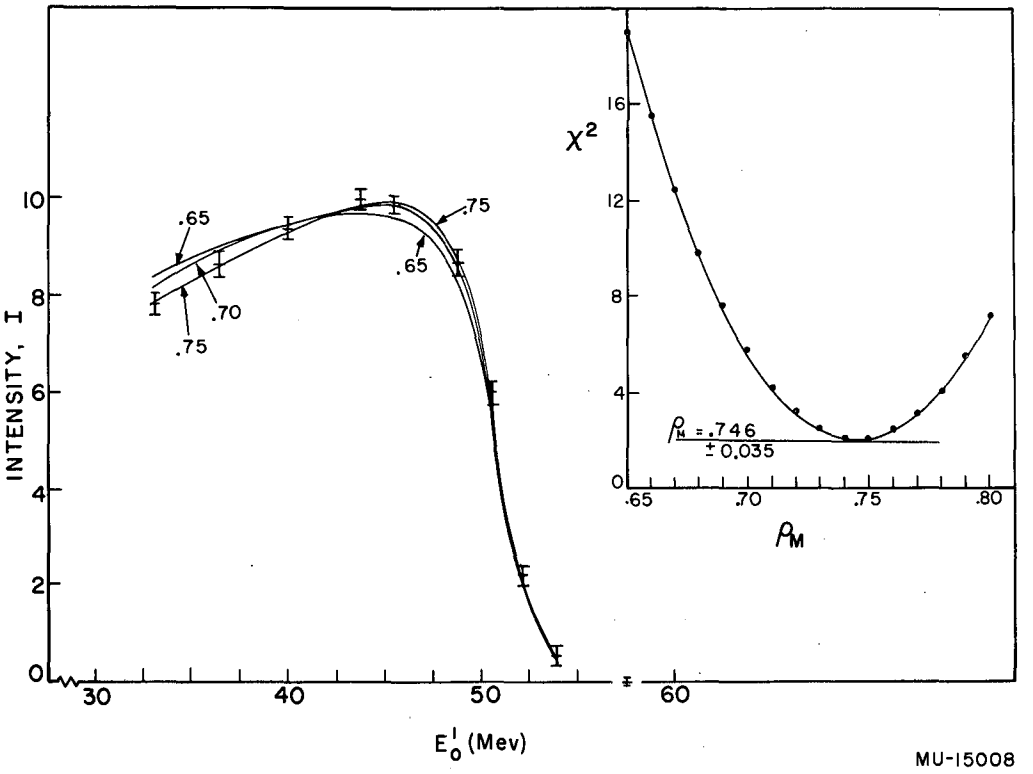

Fig. 8. (left) Comparison of the reduced data for the stated spectrometer geometry (at $\Theta = 35^\circ$, 2-3/8-inch lithium target) with three modified Michel curves that are normalized to the data by the minimum-χ^2 method

(right) Plot of the dependence of the calculated minimum χ^2 on the Michel parameter.

ρ_M value and its standard deviation as obtained from the data for the spectrometer geometry under consideration are also given in Fig. 8.

From the theory of propagation of errors we obtain the following expression for the error on this ρ_M value:

$$\sigma_{\rho_M}^2 = \sum_{E_0'} \left(\frac{\partial \rho_M}{\partial I}\right)^2 \sigma^2 (E_0'), \tag{8}$$

which according to Eq. (7) may be expressed as

$$\sigma_{\rho_M}^2 = 4 \sum_{E_0'} \left[\left(\frac{\partial P}{\partial \rho_M}\right)^2 - (I-P) \frac{\partial^2 P}{\partial \rho_M^2}\right] \left(\frac{\partial P}{\partial \rho_M}\right)^2 \sigma^{-2} (E_0') =$$

$$= 4 \sum_{E_0'} \left(\frac{\partial^2 \chi^2}{\partial \rho_M^2}\right)^{-2} \left(\frac{\partial P}{\partial \rho_M}\right)^2 \sigma^{-2} (E_0'). \tag{9}$$

It should be noted that the uncertainty contribution that results from the presence of the second Michel parameter (Eq. (3)) is not included in this expression for the error in the best ρ_M value. In addition we omit the very small error that arises from the deviation (which is approximately 3%) of the χ^2 values as obtained from the parabolic equation from the plotted χ^2 values in the neighborhood of the minimum χ^2.

Each χ^2 distribution contains a parameter $n(r - s - 1)$, which denotes the number of degrees of freedom in the distribution. For our case $n = (r - 2)$ where r represents the number of E_0' values that are summed in using Eq. (7), and s represents the number of unknown parameters that are to be estimated from our data. Since we limit ourselves to only the one unknown parameter ρ_M, then we have $s = 1$. Having the minimum value of χ^2 as given in Fig. 8 and the number of degrees of freedom (for these data we have $n = 6$ and $\chi^2_{min} = 2.05$) one can determine from published tables a probability $\mathcal{P}$ which is the probability that χ^2 should exceed its observed value. Put differently, $\mathcal{P}$ is the probability that, on repeating the series of measurements one would observe larger deviations from the expected values. In interpreting the value of $\mathcal{P}$ one may say that if $\mathcal{P}$ lies between 0.1 and 0.9 the assumed distribution very probably corresponds to the observed one, while if $\mathcal{P}$ is less than 0.02 or more than 0.98 the assumed distribution is extremely unlikely and is to be questioned. For our data shown in Fig. 8 one obtains $\mathcal{P} = 0.91$. By the above criterion this value of $\mathcal{P}$ borders on the limits of almost significant. However, one should recall that because of the serious background effect on ρ_M a conservative approach is used in dealing with the raw data (as presented in Fig. 6) by purposely increasing the values used in the computation as background errors, thus yielding larger standard errors $\sigma (E_0')$ on the measured intensities $I(E_0')$

presented in Figs. 8 and 10. Equation (7) points out that the consequence of this approach is smaller χ^2 values and therefore higher values of P. Hence according to such an approach in dealing with the data no significance is ascribed to a high value of the probability P and the data are termed acceptable by the above criterion.

At this time we would like to draw attention to the plotted measurements in Fig. 5 and 6 at $E'_0 = 48.72$ Mev, which were obtained with the geometry having an angular slit $\Theta' = 25^\circ$. These are results from an earlier ratio experiment in which measurements of the intensities at three E'_0 values were made by repeated cycling of the magnetic field setting. In both these experiments the recorded intensity is lower at this E'_0 setting than would be predicted by the cluster of neighboring points. That this intensity measurement is low in both experiments may not be a valid reason to discredit the measurements. We have spent considerable time in an attempt to give significance to this difference, for we recognize its bearing on the measured value of ρ_M. We can speculate on possible causes for this difference, although we have no proof of any of them. Because the results from this early ratio experiment have been quoted (as $\rho_M = 0.62$ without radiative correction)[10], we present them in Fig. 9.

In this figure we present the linear dependence of the ratio $P(E'_2, \rho_M)/P(E'_1, \rho_M)$ on ρ_M, where E'_1 and E'_2 represent two specific E'_0 settings. The linear plot listed as "true Michel" is that which results from the ratios that are calculated from the intensities obtained from a fold of the resolution function and the function expressed by Eq. (3) (when the parameter ψ is 0). If the parameter ψ were permitted to have the values that limit its range (of ± 1), then one would obtain two additional straight lines--one on each side of the "true Michel" line. These would not be parallel but would show a slow increase of the correction to the parameter ρ_M with increasing value of ρ_M, because of the presence of this ψ parameter. Moreover this correction is not constant, but varies with the chosen E'_0 settings.

The linear plot listed as "modified Michel" is the dependence of these ratios on ρ_M when the calculated intensities contain the radiative corrections as introduced by the previously discussed methods. These plots are not parallel to the corresponding "true Michel" linear relations, and--as the effect of the parameter ψ--they show a slow increase of the radiative correction to the value of ρ_M as ρ_M increases. Also shown is the dependence of this radiative correction on the different choices of E'_0 energies. One concludes that this correction is not constant (as it is often assumed to be) and that its variation should not be omitted in an accurate determination ($\leq 5\%$) of the ρ_M value.

---

[10] R. Sagane, W. F. Dudziak, and J. Vedder, Bull. Am. Phys. Soc. 4, 174 (1956). This value was corrected to 0.72 ± 0.05, by use of part of the data presented in Fig. 10, during the presentation of the paper.

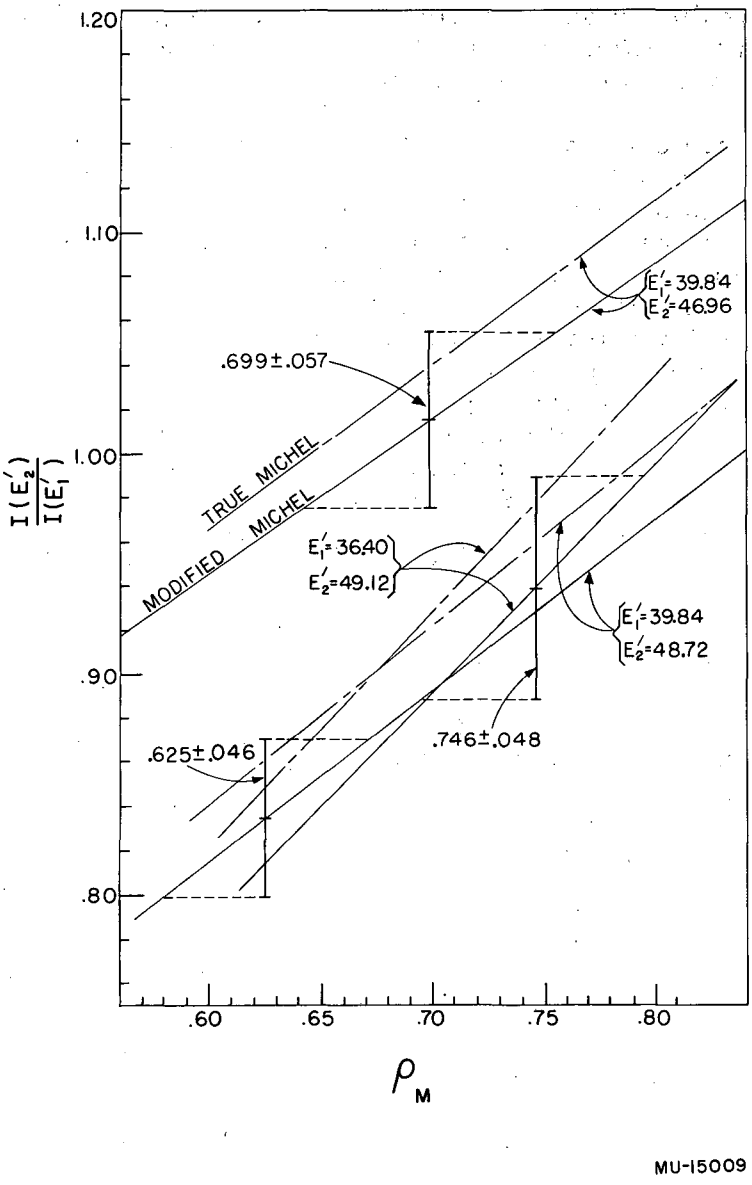

Fig. 9. Dependence of the ratio evaluated from calculated intensities at two positron energies on the Michel parameter,
(a) "True Michel," obtained by using Eq. (3);
(b) "Modified Michel", obtained by introducing radiative corrections (Eq. (4)).

In our ratio experiment we have measured the intensities at the three E_0' values of 39.84, 46.96 and 48.72 Mev. In Fig. 9 we show the two independent ratios that result from this measurement. To point out a very significant fact concerning the final quoted error in the Michel ρ_M parameter (which was once overlooked by us, and probably by others who use this method to establish the final error on ρ_M), we plot a third independent ratio measurement, which arises from the data at two E_0' values presented in Fig. 10. These ratios are plotted on the "modified Michel" linear relation to take account of the radiative correction. The extremities of the standard deviations on these ratios are projected until they intersect the corresponding linear plot. The points of intersection define the quoted errors of the ρ_M values in this plot.

If one determines the weighted mean ρ_M value and its error from these three values one obtains $\rho_M = 0.69 \pm 0.029$. This is the result from five of the intensity measurements shown in Fig. 10. If one includes the results from all the additional independent ratios that arise from the remaining intensities as given in Fig. 10, the mean ρ_M value becomes 0.72, as is also shown in Fig. 10. However, the error is approximately 0.02, or much less than the quoted error in Fig. 10, which arises from the same data by use of Eq. (9). To explain this significant difference in the estimated error by the two methods there is at least one argument that can be cited. In estimation of the error, the χ^2-test method takes into account a test of the data for internal and external consistency.[5] The test for external consistency (i.e., test for possible systematic error in the plotted data in addition to the usual accidental errors) is omitted in determination of the weighted mean error by the ratio method when the weighting factor is inversely proportional to the square of the standard deviation.

It should be noted that the square of the error of each ρ_M value as determined by the ratio method is given by

$$\sigma_{\rho_M}^2 = (\partial \rho_M / \partial_R)^2 \, \sigma_R^2 ,$$

where R is the ratio of the experimentally measured intensities at two E_0' values. In establishment of this error at a point (i.e., at each ρ_M value as shown in Fig. 9), the assumption is made that one may replace $(\partial \rho_M / \partial_R)$ by $(\partial \rho_M / \partial_Q)$, where Q is the ratio as determined from the theoretically calculated intensities.

We now apply Eq. (7) and (8) to analysis of the data for our second experimental geometry, as shown in Fig. 10, and also present the results of these analyses in Fig. 10. In our discussion of Fig. 9 we have shown the severe effect on the ρ_M value that has been introduced by the plotted intensity measurement at $E_0' = 48.72$ Mev, which arose from an earlier experiment. Because of this we analyze these data for the most likely ρ_M value, under the following conditions. We consider for Case (a) all measured values for that geometry (12 degrees of freedom) and for Case (b) all measurements after discarding the data obtained during the ratio experiment (11 degrees of freedom). Because the probability P for both these analyses lies well within the acceptance criterion, we cannot discard the

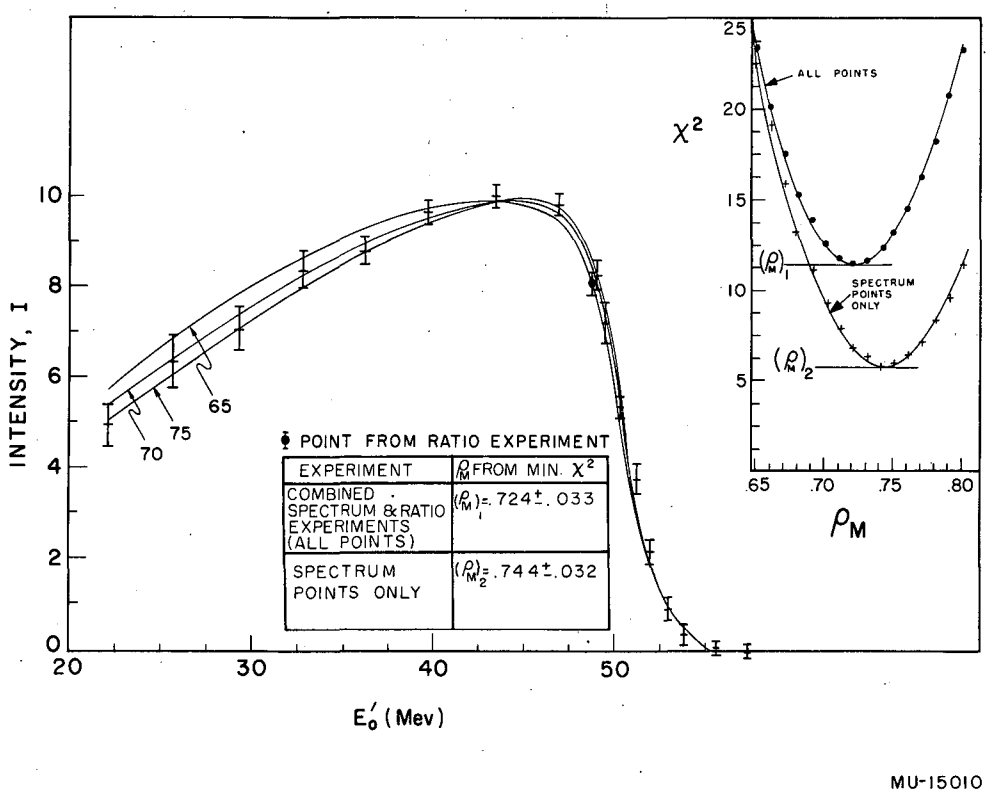

Fig. 10. (left) Comparison of the reduced data for the stated spectrometer geometry (at $\Theta = 25^{\circ}$, 2-3/8-inch lithium target) with three modified Michel curves that are normalized to the data by the minimum- χ^2 method

(right) Plot of the dependence of the calculated minimum χ^2 on the Michel parameter.

low measurement at $E_0' = 48.72$ Mev on the basis of these χ^2-test calculations. However, it should be remembered that the additional measurements from the later experiments greatly influence the acceptability of this measurement by such probability arguments.

Figure 11 represents the results of our reduction of the raw data shown in Fig. 5 for the $\Theta' = 35^\circ$ geometry. Also shown is the most probable ρ_M value as determined from these data. In this experiment the subtracted background was considerably larger than in the two experiments just discussed. In addition the original raw-data measurements were not so accurate. These, then, have led to the large error on the value of ρ_M as determined from this set of data. Because these arguments also hold for the raw data from the $\Theta'=25^\circ$ geometry (as presented in Fig. 5) we decided to combine the data from these two experiments and analyze them as arising from the same experiment. We are justified in our decision by the fact that the errors are large and do not warrant a consideration of the small differences that exist in the resolutions of these two geometries (see Figs. 18 and 19). We present these combined data in Fig. 12 along with the results from our calculations in treating these data.

Table III summarizes the results of our measurements of the Michel ρ_M parameter. These results are dependent on the assumptions that were used, in particular on the background as estimated by methods described in Appendix D and on the assumption that the second Michel parameter ψ is 0. Our error omits any contribution to the uncertainty of ρ_M by this second parameter. As previously stated, for $\psi = \pm 1$ an additional uncertainty of approximately 0.02 must be introduced to our measurement. In this table we present the two values that arise in discussion of the data presented in Fig. 10. Since we have no cause to disregard the ratio measurements we must accept the lower value. However, we also tabulate the higher value to illustrate our final result in case the ratio-intensity measurements should be ignored because of the presence of an unknown systematic error.

Table III

Summary of the measured ρ_M values

Experiment	Spectrometer geometry		ρ_M	$\sigma\rho_M$	/ ρ_M	$\sigma\rho_M$
	Lithium target diameter (inches)	Angular slit (degrees) Θ'				
1	2- 3/8	35	0.746	0.035	0.746	0.035
2	2-3/8	25	0.724	0.033	0.744	0.032
3	1	35	0.735	0.056	0.735	0.056
4	1	25				
Weighted mean value			0.734	0.022	0.743	0.022

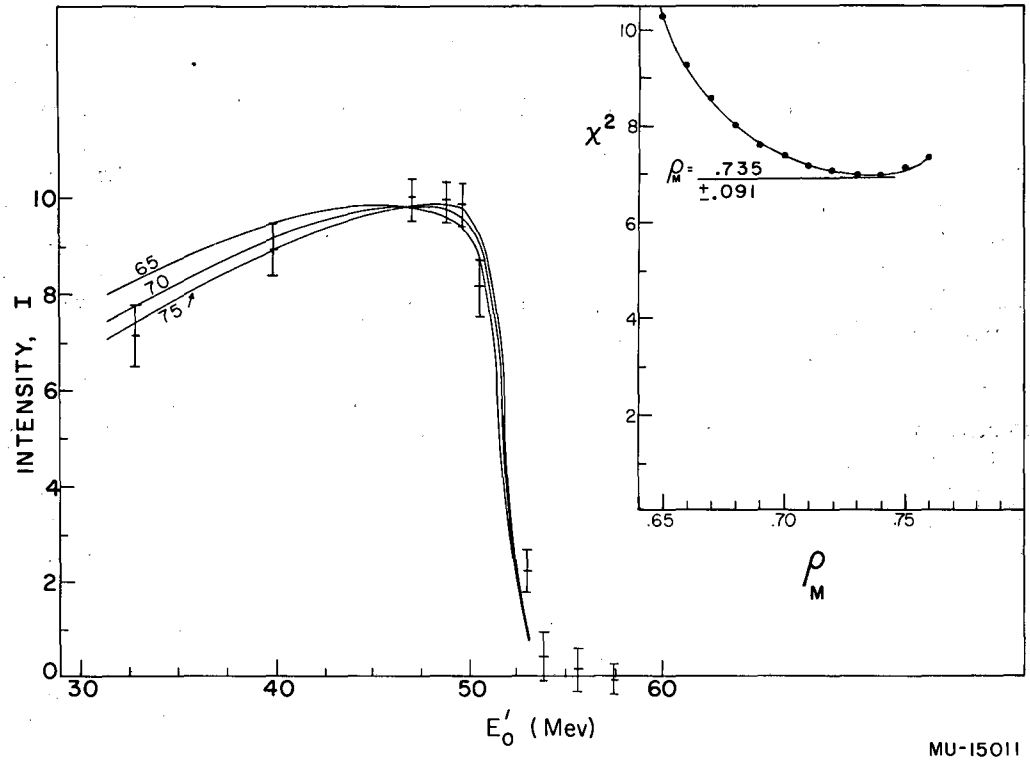

Fig. 11. (left) Comparison of the reduced data for the stated spectrometer geometry (at $\Theta = 35^o$, 1-inch lithium target) with three modified Michel curves that are normalized to the data by the minimum-χ^2 method

(right) Plot of the dependence of the calculated minimum χ^2 on the Michel parameter.

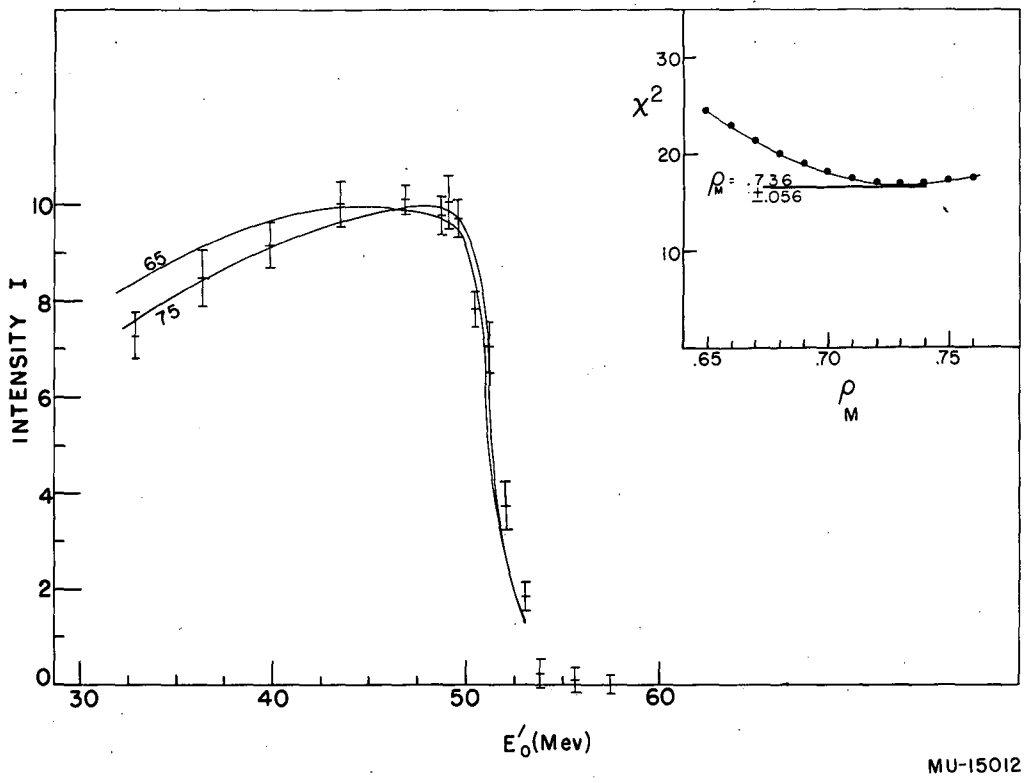

Fig. 12. (left) Comparison of the reduced data (combined for $\Theta = 25^\circ$ and $\Theta = 35^\circ$, 1-inch lithium target) with two modified Michel curves that are normalized to the data by the minimum- χ^2 method

(right) Plot of the dependence of the calculated minimum χ^2 on the Michel parameter.

MEASUREMENT OF THE MUON REST MASS

A measurement of the maximum positron energy W is also a measure of the muon rest mass μ, because of the relation between these two quantities and the known electron mass ϵ that is given by $W = (\mu^2 + \epsilon^2)/2\mu$. As shown in Figs. 8 and 10 the separation of the different ρ_M curves is very small near the cutoff because of the steep slope that occurs in this positron energy region. The steepness of the slope for a set of Michel curves that are within a ρ_M interval of $\pm$ 0.05 is determined primarily by the resolution of the spectrometer. One may use this strong dependence of the shape of the positron spectrum on the spectrometer resolution to measure the value of W without knowing precisely the value of the Michel parameter ρ_M.

In our experiment we have used three different targets as the primary means of change in spectrometer resolution. For each of these three targets we determined the resolution of our spectrometer. Using the modified Michel equation that arises from Eq. (4) for $\rho_M = 0.73$, we calculated the expected family of theoretical intensities for different W values and for each resolution by the folding procedure we previously described. If these calculations for each spectrometer resolution were plotted, they would represent a family of steeply varying curves, each indicating a different W cutoff energy.

The data from the three experiments are presented in Fig. 13. The plotted data illustrate the strong effect of spectrometer resolution on the Michel spectrum near the maximum positron energy. Because normalizations are involved in presenting these data on one plot, this illustration should be treated as qualitative. Each set of data is analyzed separately and we give quantitative significance only to this analysis.

We analyze each experimental set of measurements by the minimum-χ^2 method that we previously described. To do this we rewrite Eq. (7) after replacing ρ_M by W so that we have

$$\chi^2 = \sum_{E_0'} \sigma^{-2}(E_0') \left[I(E_0') - P(E_0', W) \right]^2 .$$

As an illustration, a curve connecting the predicted calculated intensities at one W value, normalized by determination of the minimum χ^2 at this W value, is also plotted in Fig. 13 for one set of measurements (lithium target). The most probable value of W is determined from the minimum χ^2 obtained by setting equal to zero the first derivative of the fitted parabolic equation representing the calculated minimum χ^2 values as a function of W. To determine the standard error on this W measurement we use the expression

$$\sigma_W^2 = 4 \sum_{E_0'} \sigma^{-2}(E_0') \left(\frac{\partial P}{\partial W} \right)^2 \left[\frac{\partial^2 \chi^2}{\partial W^2} \right]^{-2} .$$

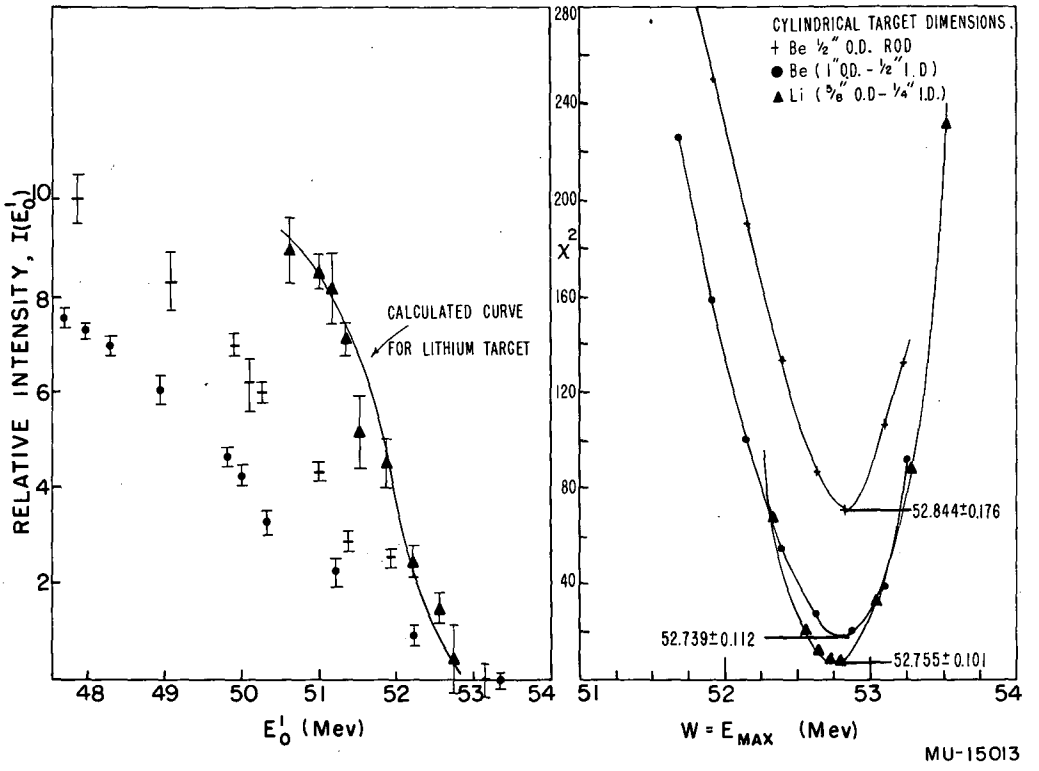

Fig. 13. (left) Reduced experimental data as obtained for three different spectrometer resolutions in a study of the maximum positron energy.

(right) Plot of the dependence of the calculated minimum χ^2 on the maximum positron energy for each set of data.

The results of our calculations are shown in Fig. 13 and are also summarized in Table IV. The very high χ^2 values for the experiment using a Be target ($\frac{1}{2}$-inch diameter) are a direct result of the high measured intensity at $E_0' = 52$ Mev.

Because these measurements have been made in air, a small energy correction is necessary in the energy scale to account for positron energy loss in air. (This correction was included in the energy scale of the previously discussed data.) To establish the most probable path length in air we have used the data from our α-particle studies on the resolution of a spiral-orbit spectrometer. One phase of these studies involved positioning a well-collimated line source of monoenergetic α particles at a fixed radius and measuring the intensity and shape of the resolution at the detector by varying the magnetic field. The line source was rotated after each measurement (i.e., θ was varied and r_0 was constant) until measurements were made for angles covering a complete 360° rotation of the line source. From these data an experimentally measured curve of collection probability as a function of angle of emission with respect to the α-particle detector was determined. Each angle of emission corresponds to a particular path length (Fig. 2). From these relations a most probable path of positrons in air was determined. Following the procedures outlined in Appendix A, we have calculated the most probable energy loss by using Sternheimer's results for nitrogen and oxygen. These calculations yield an 0.11-Mev correction to the measured value of the maximum energy. Adding this correction to the weighted mean value appearing in Table IV, we obtain $W = 52.87 \pm 0.069$ Mev for the most probable value of the maximum positron energy. From this value and its simple algebraic relation to the masses of the decay particles we obtain $\mu = (206.94 \pm 0.27)\epsilon$ for the most probable muon rest mass.

Table IV

Summary of the measured maximum positron energy W

Experiment No.	Spectrometer Target Element	Spectrometer Target External and Internal Diameters (inches)	W (Mev)	σ_W (Mev)
1	Li	$\left(\frac{5}{8} - \frac{1}{4}\right)$	52.755	0.101
2	Be	$\frac{1}{2}$ (solid)	52.844	0.175
3	Be	$\left(1 - \frac{1}{2}\right)$	52.739	0.112
Weighted mean value			52.763	0.069

ACKNOWLEDGMENTS

We should like to acknowledge the interest of Dr. Walter Barkas and helpful discussions with Professor Edwin McMillan during the course of this experiment. In particular we should like to express our gratitude to Dr. Alper Garren and Dr. Warren Heckrotte for their efforts in making an independent study of the resolution of our spectrometer during the earlier stages of the experiment. We should also like to acknowledge the invaluable help of Mr. Michael Lourie in the programming of the tedious computations on the IBM computer. Finally we should like to express our appreciation to Mr. James Vale and the entire cyclotron crew for efficient operation of the cyclotron during the experiment.

This work was done under the auspices of the U. S. Atomic Energy Commission.

APPENDIX

A. Ionization and Straggling; Spectrometer Resolution

The resolution of the spectrometer was obtained by use of an IBM 650 machine and numerical calculations as follows.

The radius of the cylindrical target was subdivided into fifteen equal segments. The circular boundaries of these radial segments defined a target volume. In what follows let r_0 represent the mean radius of any one of these fifteen cylindrical segments. For each radius r_0 a probability-of-occurrence function of a straight-line path length t through the target was determined. This probability-of-occurrence function results from a numerical calculation of the angle subtended by a path length t and t + Δt, where Δt was set equal to 0.005 inch. According to the procedure of C. N. Yang,[11] the most probable path length ℓ for an electron was calculated from each straight-line path length t, by use of the simplified expression $\ell = t(1 + \frac{t}{\lambda})$ where λ is the characteristic scattering length. We used the result as obtained by W. T. Scott[12] for the definition of λ, which is

$$\frac{1}{\lambda} = \frac{2\pi e^4 Z^2 N}{p^2 v^2} \ell n \frac{150\, pc}{mc^2 Z^{1/3}} ,$$

where m, p, v, e are the mass, momentum, velocity, and charge of the electron, c is the velocity of light, Ze the charge of the scattering nucleus, and N the number of nuclei per cm^3. This calculation procedure yielded fifteen separate probability-of-occurrence functions $P(\ell, r_0)$ (one for each r_0) of the most probable path lengths for electrons originating in the cylindrical volume segment defined by a differential radial element at a radius r_0. (For example see Fig. 14.)

A monoenergetic beam of electrons of energy E_0 after traveling a certain path length ℓ in material, loses energy by ionization and radiation processes. The probable energy distribution of an initially monoenergetic electron beam that results from collision losses after it has traveled a path length ℓ through matter has been calculated approximately by Landau[13] and more recently by Shultz,[14] Blunck and Leisegang,[15] and Symon.[16] We

---

[11] C. N. Yang, Phys. Rev. 84, 599 (1951).

[12] W. T. Scott, Phys. Rev. 76, 213 (1949).

[13] L. Landau, J. Phys. (U. S. S. R.) 8, 201 (1944).

[14] W. Shultz, Z. Physik 129, 530 (1951).

[15] O. Blunck and S. Seisegang, Z. Physik 128, 500 (1950).

[16] K. R. Symon, Thesis, Harvard University 1948 (Unpublished).

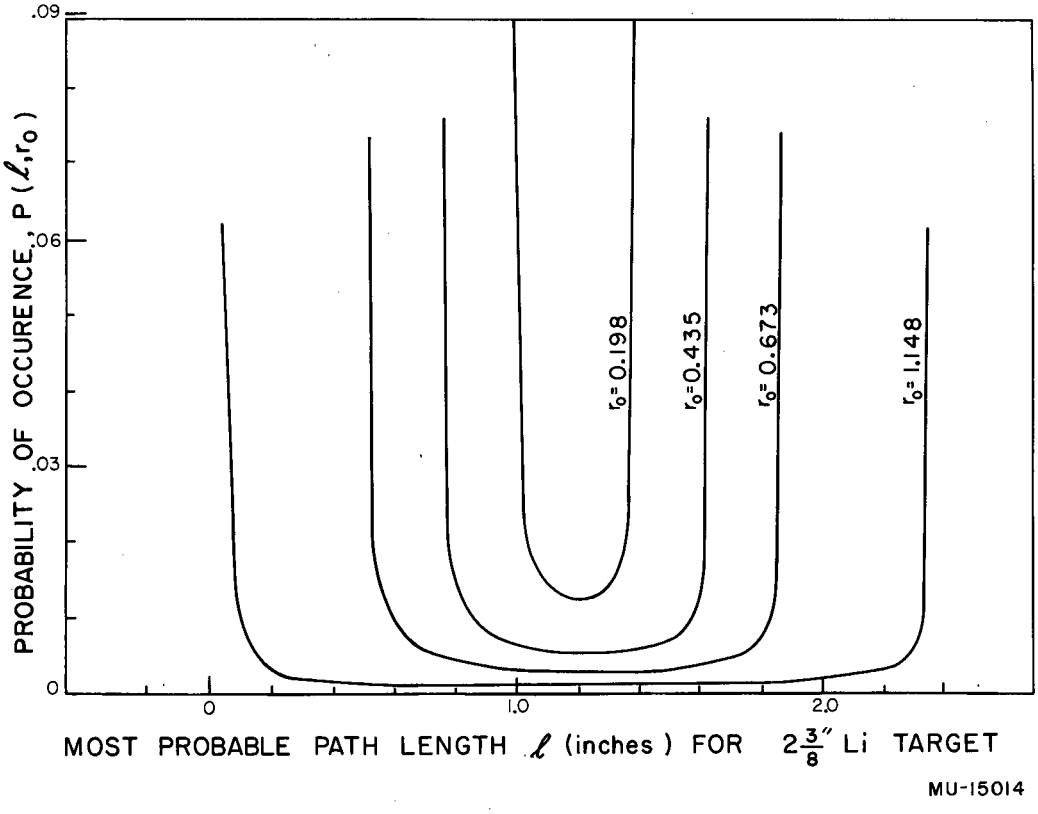

Fig. 14. Calculated probabilities of the most probable positron path length ℓ in a solid cylindrical lithium target as a function of target radius r_0.

find that the analytic expression given by Blunck and Leisegang for this energy distribution would be very useful in our type of calculation. However, calculations reveal that the full width at half height of the energy-distribution function that is obtained by use of their results is smaller by 7% than that given by Symon. Since Symon's results are in excellent agreement with the experimental data of Goldwasser, Mills, and Hanson,[17] we have used his data to represent what is normally referred to as the Landau distribution in our work. In addition we have extended the tail of his calculated probability distribution from abscissa values $(\Delta - \epsilon_p)/\Delta_0 = 10$ to 15 by Landau's derived inverse-square behavior for this region.

For an initial electron energy E_0 associated with each electron path length ℓ (cm) there is a probable electron-energy (or Landau) distribution $L(\ell, \Delta)$, and also a most probable electron energy loss ϵ_p. The most probable energy loss ϵ_p was obtained by using the Sternheimer expression,[18]

$$\epsilon_p = \frac{2\pi NZe^4}{mv^2} \ell \left[\ell n \frac{2mv^2 (2\pi NZe^4 \ell / mv^2}{I^2 (1-\beta^2)} - \beta^2 + 0.37 - \delta \right],$$

which can also be written as

$$\epsilon_p = \Delta_0 \left[B + 1.06 + 2 \ell n \frac{p}{mc} + \ell n \frac{A\rho' \ell}{\beta^2} - \beta^2 - \delta \right],$$

where $\Delta_0 = \frac{A\rho' \ell}{\beta^2}$, and where ρ' is the density of target material (g/cm^3), A and B are tabulated constants as presented in (18a), and δ is given approximately by an analytic expression. For lithium we used

$$\delta = 4.606\, X - 3.07 + 0.374\, (X, -X)^{3.05}, \quad (\text{for } X < 2)$$

$$\delta = 4.606\, X - 3.07, \quad (\text{for } X > 2)$$

$$X = \log_{10} (p/mc).$$

In addition the electron loses energy by radiation in passing through matter. To take account of this radiation correction we use the results of Bethe and Heitler[19] to modify each Landau distribution in the following manner. Consider each ordinate $L_i(\ell, \Delta_i)$ of a normalized Landau probability distribution ($\int_{E_0}^{0} L(\ell, \Delta)\, d\Delta = 1$)

---

[17] E. L. Goldwasser, F. E. Mills, and A. O. Hanson, Phys. Rev. 88, 1137 (1952).

[18] R. M. Sternheimer, Phys. Rev. 103, 511 (1956); Phys. Rev. 91, 256 (1953).

[19] H. Bethe and W. Heitler, Proc. Roy. Soc. A. 146, 83 (1934); W. Heitler, Quantum Theory of Radiation (Oxford University Press, London, 1954), 379.

that results only from ionization losses, for a monoenergetic electron beam of energy E_0 traversing matter and having the most probable electron path length ℓ. We have $\Delta_i = (E_0 - E_i)$ which represents the corresponding electron energy loss due to ionization only. Each ordinate $L_i(\ell, \Delta_i)$ must first be modified by $W(\ell, E_i)$, i.e., by the probability that an electron still has approximately the energy E_i after radiation losses are also considered. To calculate $W(\ell, E_i)$ we use the Bethe-Heitler relation

$$W(b\ell, y) = \frac{(b\ell - 1, y)\ !}{\Gamma(b\ell)} \quad ,$$

i.e., the probability that an electron still has an energy greater than e^{-y} times the energy E_i after traversing the path length ℓ. The $(b\ell - 1, y)!$ is the "incomplete gamma function",[20] $y = \ell n\,[E_i/(E_i - k)]$; k is the energy loss by radiation after traversing a short distance; and b is a constant whose value depends on the density and charge of matter being considered. For lithium, b is 5.56×10^{-3} cm^{-1}. To determine $W(\ell, E_i)$ we set $k = k' = 1.28$ kev.

In addition, the Landau probability-distribution ordinates are modified by contributions from those electrons that experience radiation losses, i.e., $[1 - W(\ell, E_i)]\, L_i(\ell, \Delta_i)$. Because of radiation losses there is a shift of electrons from the higher E_i energies to lower electron energies, resulting in an increase of the $W(\ell, E_i)\, L_i(\ell, \Delta_i)$ probability ordinates for lower E_i energies. To determine $\delta L_j(\ell, E_j)$ (that is, the amount of this increase in a particular probability ordinate that corresponds to an energy E_j), we use the expression

$$\delta L_j(\ell, E_j) \cong \sum_i [1 - W(\ell, E_i)]\, \Delta w(y_{ij})\, L_i(\ell, \Delta_i)$$

where the summation over i is the contribution of all electron energies $E_i > E_j$, and y_{ij} is the value of y obtained for a particular energy loss through radiation $k_{ij} = (E_i - E_j)$. For w(y) we use the Bethe-Heitler expression

$$w(y) = \exp(-y)\, y^{(b\ell - 1)} / \Gamma(b\ell) \, ,$$

which represents the probability that the energy of an electron that has traversed a finite distance ℓ has decreased by the factor e^{-y}. In all our calculations we normalize by setting w(y) = 100% for $k = k' = 1.28$ kev. $\Delta w(y_{ij})$ is defined as the difference between two values of w(y) evaluated for $k = E_i - E_j$ (in Mev) and $k = (E_i - E_j - 0.00128)$. (In these calculations we use a fixed energy mesh of 0.04 Mev.)

The Landau probability ordinates modified to take into account electron radiation losses are given by the sum $[W(\ell, E_j)\, L(\ell, E_j) + \delta L_j(\ell, E_j)]$ for each most probable path length ℓ and initial electron energy E_0. In

[20] K. Pearson, Tables of the Incomplete Γ - Function (Cambridge University Press, Cambridge, England 1946).

addition, this sum must be multiplied by the probability of occurrence, $P(\ell, r_0)$, of the path length ℓ for the differential volume segment designated by r_0. Four of the fifteen probability functions $P(\ell, r_0)$ are illustrated in Fig. 14. These are normalized so that we have

$$\int_{\ell\ \min}^{\ell\ \max} P(\ell, r_0)\, d\ell = 1.$$

To obtain the most probable electron distribution $Q(\Delta, r_0)$ from a differential volume r_0 that results from a monoenergetic electron source the above calculations are performed for each possible ℓ value. The resulting sum of the contributions from all ℓ values yields the desired probability

$$Q(\Delta, r_0) = \int_{\ell\ \min}^{\ell\ \max} [W(\ell, k)\, L(\ell, \Delta) + \delta L(\ell, \Delta)]\ P(\ell, r_0)\, d\ell.$$

We evaluated this expression for each r_0 by approximating the integral by a sum. For the innermost first six r_0 shells a $\Delta\ell$ mesh of 0.2 mm was used. A $\Delta\ell$ mesh of 0.4 mm was used for the seventh, eighth, and ninth shells and 0.5 mm $\Delta\ell$ mesh for the remaining larger r_0 shells.

Figure 15 illustrates the function $Q(\Delta, r_0)$ for five of the fifteen different r_0 values for a lithium cylindrical target whose diameter is 2.375 inches. These $Q(\Delta, r_0)$ values represent the most probable energy distribution for electrons initially at 50 Mev, originating at a specific target position r_0, and undergoing ionization and radiation losses while emerging from the target. The areas under these curves are normalized so that we have

$$\int_{\Delta\ \min}^{\Delta\ \max} Q(\Delta, r_0)\, d_\Delta = 1$$

Consider now the magnetic focusing of these electrons when the source is centrally located in a magnetic field such that the longitudinal axis of the cylinder coincides with the magnetic axis of a spiral-orbit spectrometer. Suppose that this is the z-axis of a cylindrical coordinate system (r, θ, z) and that $z = 0$ defines the median plane of the spectrometer. One of the principal spectrometer requirements is that the magnetic field be axially symetric, that is in a cylindrical coordinate system:

$$B_r(r, z) = -B_r(-z, r);$$

$$B_\theta = 0;$$

$$B_z(r, z) = B(r, -z).$$

As illustrated in Fig. 2, equations of motion show that a charged particle originating in the cylindrical source spirals into an orbit $r = \rho$ about the z axis if the magnetic conditions are such that its radial velocity and

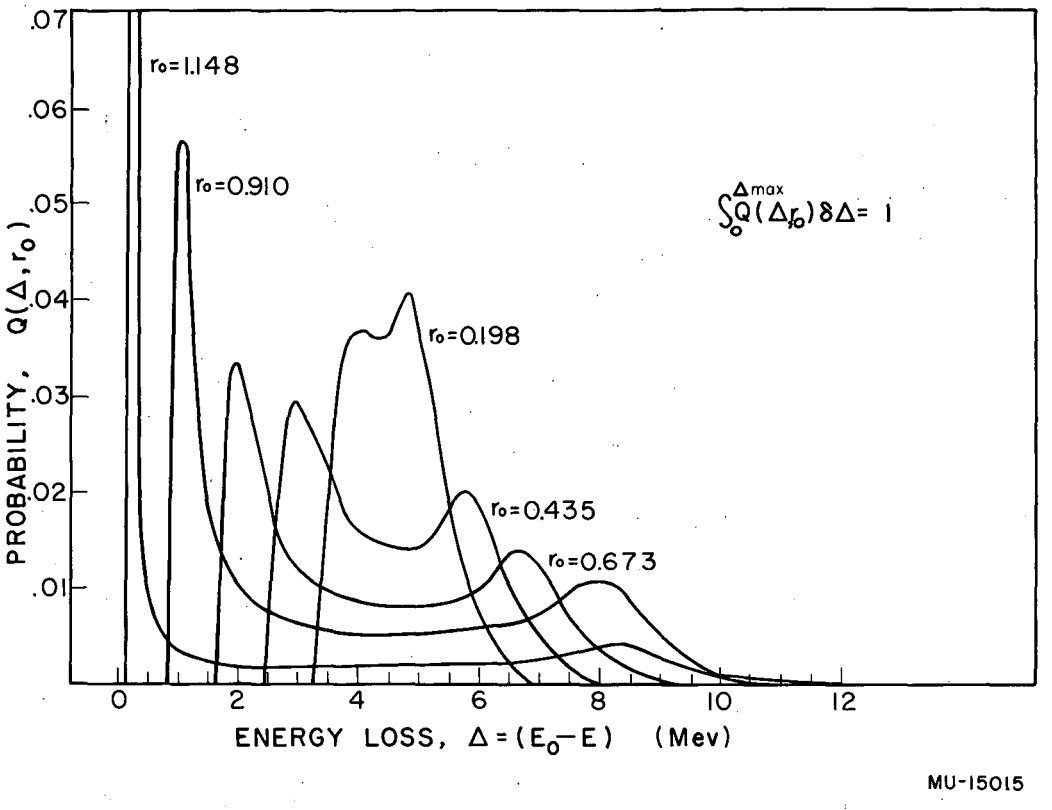

Fig. 15. Calculated radial dependence of the probabilities of positron-energy loss for a monoenergetic positron source undergoing combined ionization- and radiation-energy losses in emerging from a solid cylindrical lithium target.

radial acceleration become zero. For motion in the median plane these requirements state[3] that the vector potential is at a maximum at $r = \rho$ and that the following relations exist between the vector potential, magnetic field, and radius ($r = \rho$) of the circle of convergence at $r = \rho$:

$$A(\rho) = B(\rho) \cdot \rho = \frac{1}{\rho} \int_0^{\rho} B(r) \cdot r \, dr .$$

It was first pointed out Iwata, Miyamoto, and Kotani[3] that this expression defines a circle of convergence and that the radius ρ of this circle depends on the shape of the magnetic field strength irrespective of the absolute value of the magnetic field. Fig. 4 presents the shape (with respect to strength $B(r)$) of the radial magnetic field that was used in this experiment. It also illustrates a graphical method that can be used to determine the value of the radius ρ.

Suppose that a detector is located so that the center of the detector coincides with the circle of convergence and so that the radial dimension of this detector defines two circles, in the neighborhood of the circle of convergence, having radii equal to $\rho + d$ and $\rho - d$. Particles whose spiral paths pass through the inner circle can be detected. The probability of detection for these particles varies between zero and one. It depends on the length of the spiral path within the annular region defined by the two circles of radii $\rho + d$ and $\rho - d$. This portion of the path length can best be measured by the central angle Θ that it subtends. For all practical purposes the detection probability is unity for all particles whose paths are within these radial boundaries and whose central angles are $> 2\pi$, since these are lost after passing through the detector for the first time.

Consider now a monoenergetic source located concentric to the axis of magnetic symmetry at a radius r_0. Suppose that the source intensity is independent of the angle of emission α. Under these conditions it can be shown[3] that to a very good approximation the subtended central angle is given by

$$\Theta \simeq \kappa \sqrt{2} \cosh^{-1} (\mu + \epsilon \sin \alpha)^{-0.5}$$

for $(\mu + \epsilon \sin \alpha) > 0$, (Case 1)

$$\Theta \simeq \kappa \sqrt{2} \sinh^{-1} (|\mu + \epsilon \sin \alpha|)^{-0.5}$$

for $(\mu + \epsilon \sin \alpha) < 0$, (Case 2)

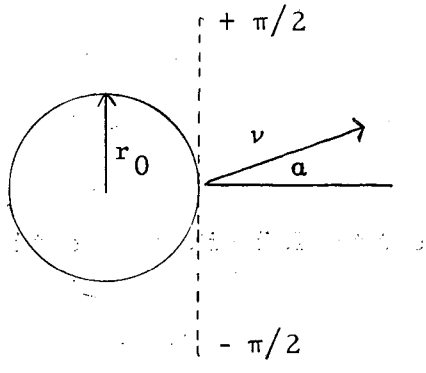

where κ is a constant obtained from the shape of the magnetic field at the focus orbit,

$$\mu = \kappa^2 \cdot \frac{\Delta B}{B} \cdot \frac{\rho^2}{d^2} ,$$

$$\epsilon = \kappa^2 \cdot \frac{r_0}{\rho} \cdot \frac{\rho^2}{d^2} ,$$

and κ is related to the more familiar field parameter $n = -\frac{r}{B}\frac{dB}{dr}$ by the expression $\kappa = \sqrt{2/(n-1)}$. Case 1 represents all particles that do not have sufficient momenta to escape from the region of the magnetic field. Case 2 applies to all particles whose momenta are such that they can escape from this region.

The resolution of a homogeneous monochromatic source located at r_0 is given by the integral of Θ for all possible values of α. In an experiment a detector and a slit system located so that the defining edge is at a radius $r = \rho - d$ subtend a central angle Θ'. This angular width Θ' of the detecting system limits the actual number of detectable particles as given by Θ. For such a system the resolution of the spectrometer is given by

$$I(\mu, \epsilon, \Theta') = \frac{1}{2\pi^2} \int_{-\pi/2}^{\pi/2} (\Theta - \Theta') \, d\alpha, \quad \text{for } \Theta \geq \Theta' ,$$

and $$I(\mu, \epsilon, \Theta') = 0, \quad \text{for } \Theta < \Theta' .$$

In our experiment Θ' had two values, $\Theta' = 25^\circ$ and $\Theta' = 35^\circ$. We have numerically evaluated these integrals for the two values of Θ' by the following simplified procedure. Given Θ', μ, and ϵ, we used Simpson's 1/3 rule with a $\Delta\alpha$ mesh of 1 degree. As previously mentioned, proper care was taken in evaluating the region $2\pi \leq \Theta \leq \infty$.

Figure 16 illustrates the intensity distribution function $I(\mu, \epsilon, \Theta') / \kappa\sqrt{2}$ for four of the fifteen different r_0 or ϵ values as obtained for $\kappa = 0.90$ and $\Theta' = 35^\circ$. These curves are again replotted in more conventional units in Fig. 17. For each r_0 the total momentum width of the intensity distribution is limited by the angular width Θ' and can be calculated from the expression

$$-\left[\epsilon + \operatorname{csch}^2\left(\frac{\Theta'}{\kappa\sqrt{2}}\right)\right] \leq \mu \leq \left[\epsilon + \operatorname{sech}^2 \frac{\Theta'}{\kappa\sqrt{2}}\right].$$

These calculations are for trajectories in the median plane. They are applicable only to such trajectories and to those that closely approximate this motion. Therefore cylindrical copper electron stoppers (2 inches thick and 30 inches i.d.) were used to limit the aperture above and below the median plane to $z = \pm 1.5$ inch. These are shown in Fig. 1. This limitation of aperture, plus the fact that the magnetic field strength is very flat (up to r = 15 inches), permits us to use these curves as good approximations for the magnetic focusing properties of the spectrometer. We have verified this experimentally by studies with monoenergetic alpha particles (and will present these results in a forthcoming paper).

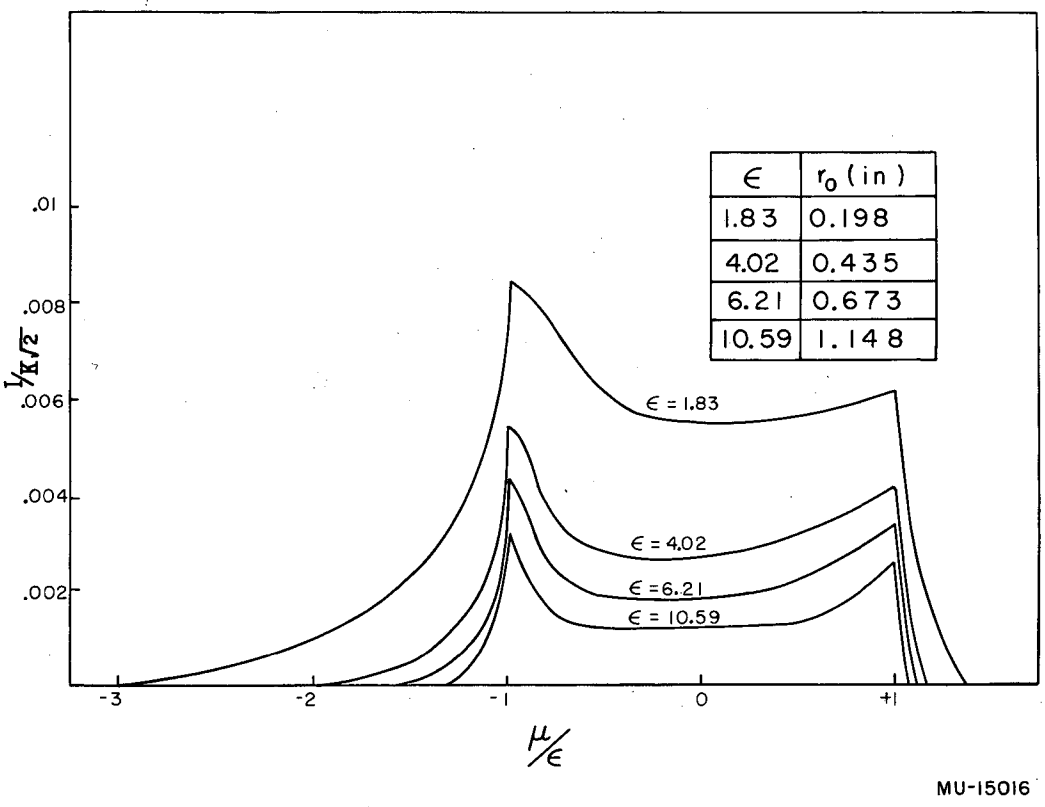

Fig. 16. Dependence of resolution on parameters of a spiral-orbit spectrometer (referred to μ/ϵ) $\Theta = 35^{\circ}$, K = 0.90, 2-3/8-inch Li target.

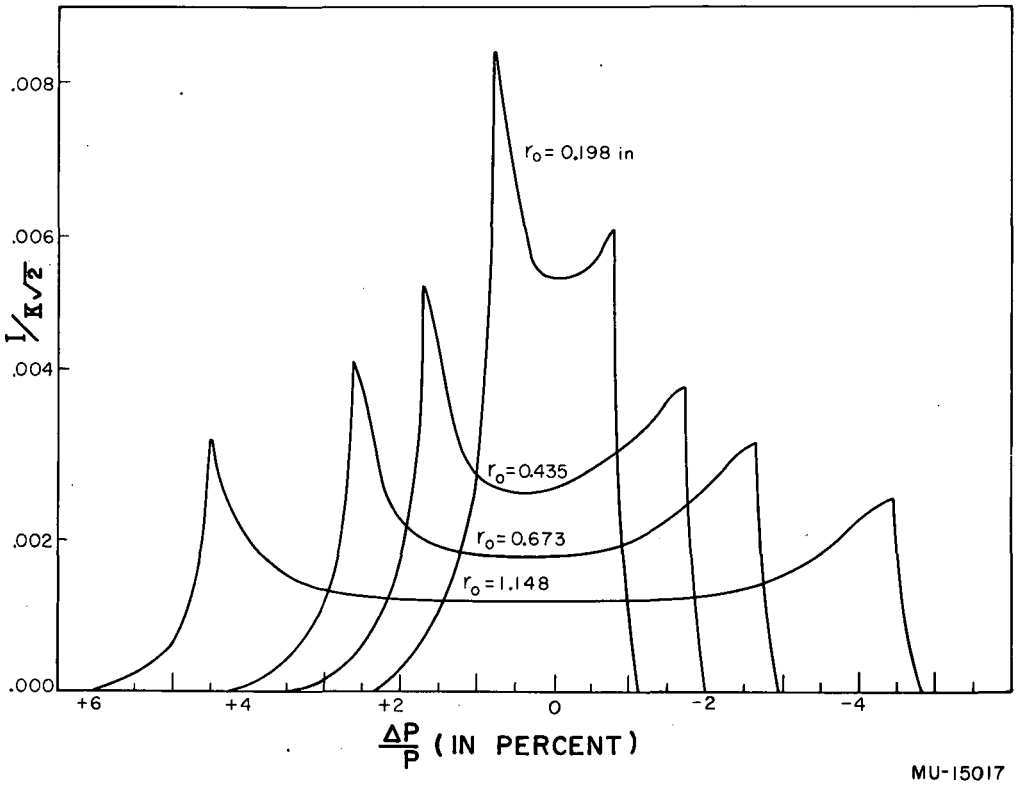

Fig. 17. Dependence of resolution on parameters of a spiral-orbit spectrometer (expressed in terms of momentum) $\Theta = 35^{o}$, K = 0.90, 2-3/8-inch Li target.

Having determined the Q and I distribution functions, we can, now calculate the function $R(E_0', \Theta', E)$, which represents the spectrometer resolution for electrons that are initially born in a cylindrical target with an energy E lose energy by radiation and ionization, and are brought to a focus at the detector of angular width Θ' by a magnetic field strength set so that the $B\rho$ value of the focus orbit is a measure of an electron energy E_0'. We obtain $R(E_0', \Theta', E)$ by a series of numerical calculations whereby we approximate the integral over r in the expression

$$R(E_0', \Theta', E_0) = \int_0^{r\ max} F(E_0', E_0, \Theta', r_0)\, W(r_0)\, d r_0 =$$

$$= \int_0^{r\ max} W(r_0)\, d r_0 \int_0^{E_0} I(E_0', \Delta E', \Theta', r_0)\, Q(E_0 \Delta E, r_0) dE$$

by a summation of fifteen different r_0 shells. Here $W(r_0)$ is the volume-weighting factor. The integral determining the function F is approximated by numerical calculations, in which 0.04 Mev is used as a ΔE mesh for each E_0 value. Neighboring E_0 values differ by 0.08 Mev.

Figures 18 through 21 summarize the results of these calculations for the four different geometries that were used in this study of the Michel ρ_M parameter. These are the resolution curves that were used when the magnetic field strength was such that the focus-orbit positron energy E_0' was 50 Mev. Therefore they represent the resolutions of our spectrometer for the specified geometries near the maximum positron energy that is possible in the muon decay. Also shown are the variations with magnetic setting of the focus-orbit energy E_0' and the energy E_2 of the peak of the resolution, from the energy E_1 at which the half area of the resolution occurs. These illustrate the point that the simple magnetic-spectrometer property ($\Delta P/P$ equals a constant) no longer holds. This arises from the fact that positron ionization and radiation losses do not have the same momentum dependence as the magnetic focusing properties of the spectrometer. We find that one can closely approximate the shape of the proper resolution at other E_0' energies from the illustrated resolution curve by using the linear relations between these variations along with three other relations. For the geometry of the spectrometer ($\Theta' = 35^\circ$; 2-3/8-inch diameter lithium target) the additional relations are as follows:

(a) The area under the resolution curve, divided by $B\rho$ of the focus orbit at the desired energy E_0', equals a constant.

(b) The $(\Delta E)_{min}$ ratio obtained from the linear relation

$$(\Delta E)_{min} = (E_2 - E_{min}) = 0.0576\ E_0' + 1.528$$

is used to modify the ΔE intervals on the low-energy side of the half-area energy E_2 of the resolution curve. Here E_{min} is the low-energy cutoff of the resolution curve.

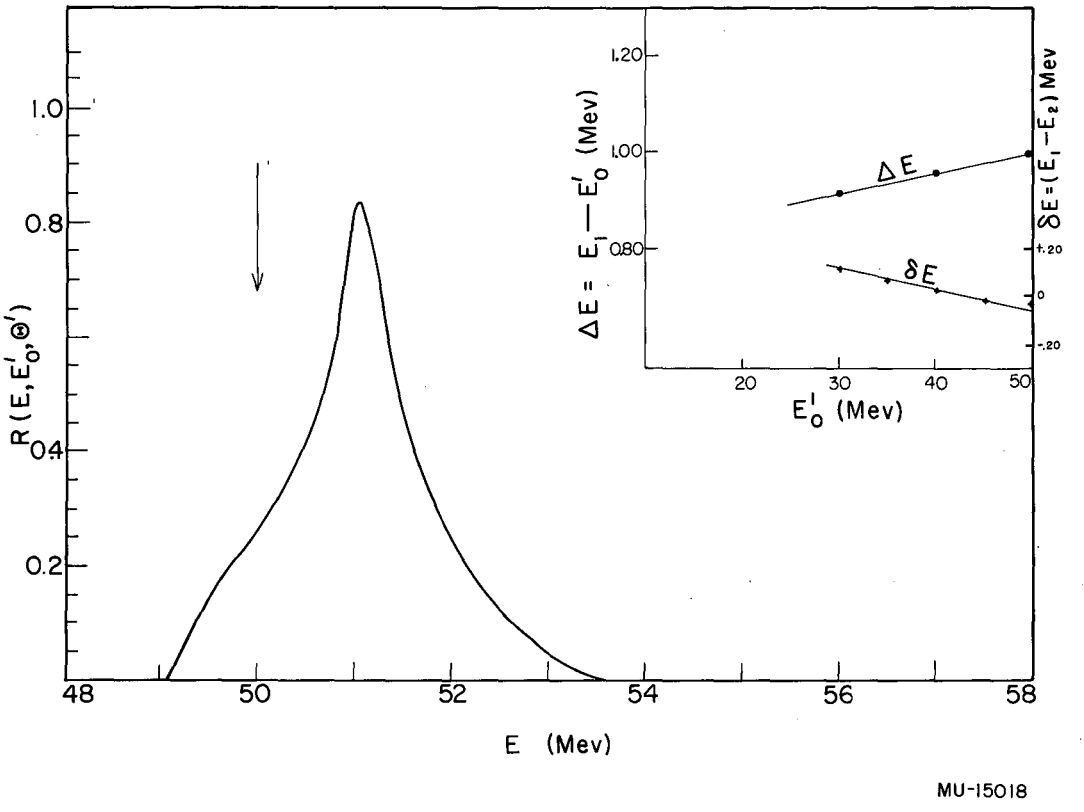

Fig. 18. Combined resolution for positrons having a focus energy of 50 Mev for $\Theta = 35^{\circ}$, K = 0.90, 1-inch Li target.

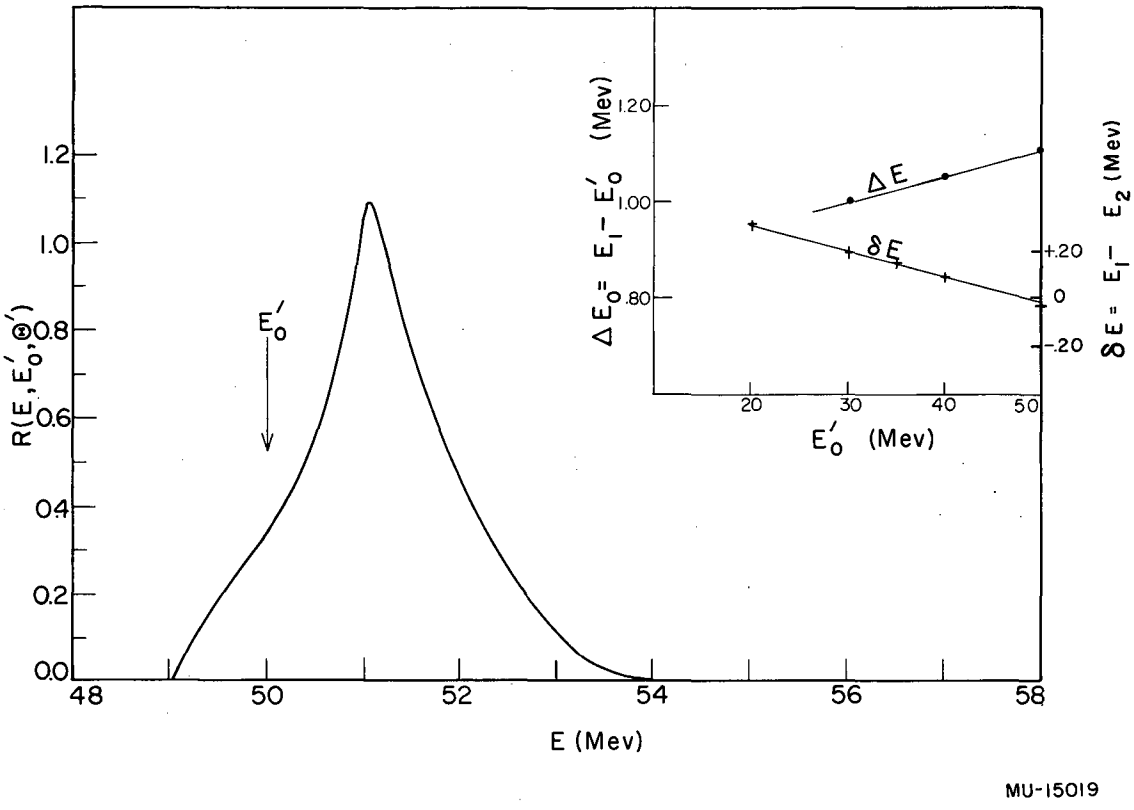

Fig. 19. Combined resolution for positrons having a focus energy of 50 Mev for $\Theta = 25^{o}$, K= 0.90, 1-inch Li target.

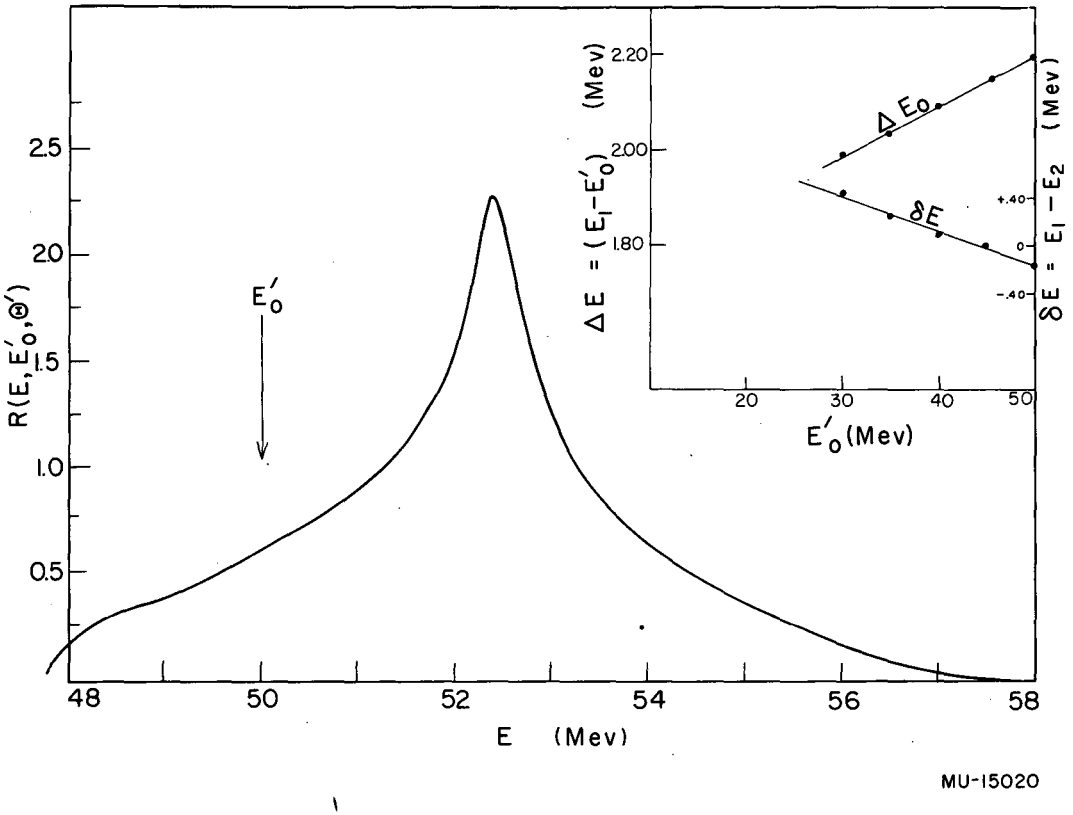

Fig. 20. Combined resolution for positrons having a focus energy of 50 Mev for $\Theta = 35^{\circ}$, K = 0.90, 2-3/8-inch Li target.

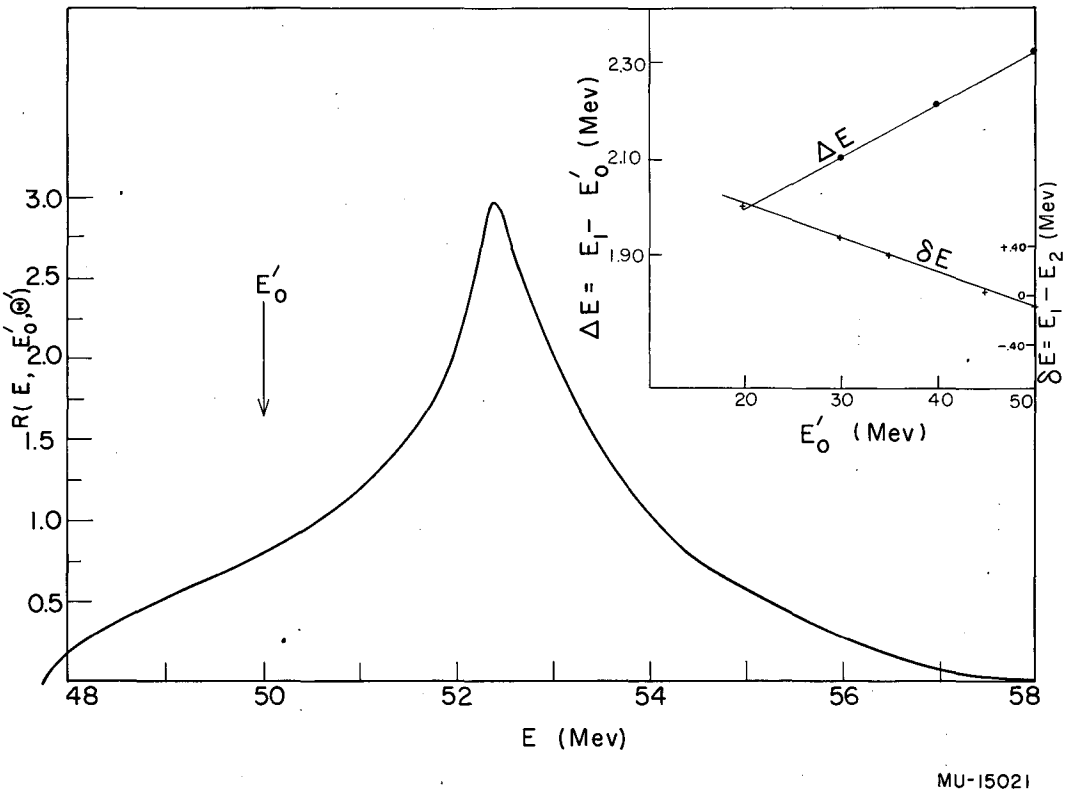

Fig. 21. Combined resolution for positrons having a focus energy of 50 Mev for $\Theta = 25^{\circ}$, K = 0.90, 2-3/8-inch Li target.

(c) The $(\Delta E)_{max}$ ratio obtained from the linear relation

$$(\Delta E)_{max} = (E_{max} - E_2) = 0.0499\, E_0' + 4.023$$

is used to modify the ΔE intervals on the high-energy side of the half-area energy E_2 of the resolution curve. Here E_{max} is the high-energy cutoff of the resolution curve. To conserve IBM time we have used this procedure only in special cases over a 2-Mev interval. However, we find that it gives a good approximation to the proper resolution curve over variations of ± 10 Mev. We list this procedure to permit detailed calculations of resolution curves at other energies by those desiring to test our data by possible variations of the theory as presented in this paper.

Figure 22 presents a summary of additional calculations illustrating the focusing properties of the spiral-orbit spectrometer when straggling, ionization, and radiation losses are neglected. We define the resolution $R(\Delta P/P, \Theta')$ by the integral

$$R(\Delta P/P, \Theta') = \int_0^{r_{max}} I\,(\Delta P/P, \Theta', r_0)\, W\,(r_0)\, dr_0.$$

The plotted curves are for the four geometries stated. They are the results of numerical calculations in which we approximate the integral over r by a summation of fifteen different r_0 shells. Here $W\,(r_0)$ is the volume-weighting factor.

As a final remark we would like to state that errors exist in some of the published resolution curves (Reference 3b.) Some of our earlier reductions were based on these curves.

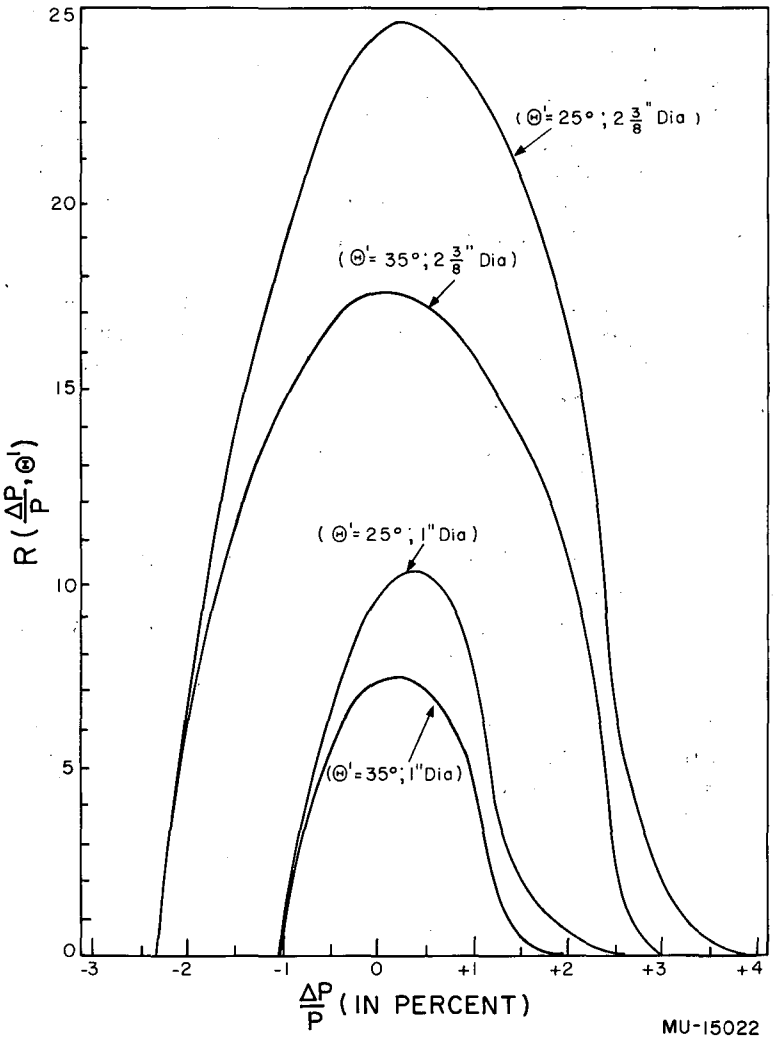

Fig. 22. Comparison of spiral-orbit spectrometer resolution for the four experimental geometries.

B. Effect of Saturation on the Michel ρ_M Parameter

When properly used, the spiral-orbit spectrometer is an instrument that yields much higher counting rates for a given resolution than other magnetic spectrometers (by a factor of from 10 to 100). Some comparisons of its properties and that of other spectrometers have already been made.[3d] One point that has not been stressed is the effect of small changes of the magnetic-field distribution on the counting rate. As has been stated, one determines the position of the focus orbit from the solution of the relation

$$A(\rho) = \rho B(\rho) = \frac{1}{\rho} \int_0^{\rho} B(r) \cdot r \, dr.$$

In our early experiments, which led to our preliminary publication of the Michel parameter as $\rho_M = 0.23$, we compared the positions of this focus orbit as obtained from two magnetic distributions.[7] The radii of these two positions were $\rho = 27.13$ inches and $\rho = 26.93$ inches. Since the radial dimension of our detectors was 3 inches, we did not attribute any significance to this difference, which corresponds to a 0.7% difference in momentum at the position of focus and is even less when the arithmetic average of these two values is used. The significance of this difference was overlooked for nearly a year, and it is this oversight that led to our publication of a Michel value of $\rho_M = 0.23$ which is in error.

The true significance of this difference was finally recognized when the large pole tips that were part of a large vacuum chamber (Fig. 4) were removed and the spectrum remeasured with poles that were the core of the magnet (Fig. 4). Because of the striking difference in the shapes of our measured positron spectrum as obtained with the two magnetic geometries, magnetic field distributions were measured at numerous positron energies (for method see Fig. 2). From these magnetic measurements it was learned that there was a systematic decrease of the focus-orbit position in the old magnetic geometry, and that this decrease resulted from a gradual change of the shape of the radial magnet field distribution. This is partially summarized in Table V, in which E_0' is the energy of the positron at the focus orbit; B_{max} is the maximum magnetic field in the median plane (which for this geometry occurs at r = 5 inches); $A(\rho)$ is the vector potential at the focus orbit; ρ is the radial position of the focus orbit and the B_r/B_{max} are the ratios of the magnetic field at the stated radii to the maximum magnetic field. For the radial magnetic-field distribution to be the same the ratios in each of the five B_r/B_{max} columns should be the same. Because the slit system remains fixed for each Θ' geometry, the decrease in the focus orbit together with the changing of the radial magnetic-field distribution constitutes an increase in resolution as positron energy is increased. This additional change in resolution caused the striking change in counting intensity that was overlooked in reporting our earlier data.

Table VI represents similar information on the new magnetic geometry that was used throughout this experiment. From this table the conclusion

can be drawn that the necessary condition that the shape of the magnetic field distribution remain the same over the positron-energy range of this experiment--has been fulfilled by our new geometry.

Table V

Summary of saturation-effects study of the old geometry. E_0', B_{max}, $A(\rho)$, ρ, and the ratio B_r/B_{max} are defined in the text.

E_0' (Mev)	B_{max} r=5.0 in. gauss	$A(\rho)$ (kilogauss -in)	(ρ) (in.)	Ratio B_r/B_{max} r=11.25 in.	r=18.25 in.	r=23.0 in.	r=25.0 in.	r=27.0 in.
45.36	7021	59.57	27.32	0.874	0.634	0.451	0.389	0.322
47.59	7403	62.50	27.13	0.873	0.632	0.446	0.383	0.316
48.74	7593			0.873	0.631	0.443	0.380	0.313
49.82	7772			0.873	0.630	0.441	0.378	0.313
50.90	7949	66.84	26.93	0.873	0.629	0.440	0.376	0.310
51.79	8101	68.01	26.86	0.874	0.628	0.438	0.374	0.307
52.79	8273	69.32	26.81	0.874	0.628	0.436	0.372	0.305
	8453			0.874	0.627	0.434	0.369	0.303
							Repeated Measurements	
45.47	7028	59.72	27.33					
52.19	8185	68.53	26.89					

Table VI

Summary of saturation-effects study of the new geometry

E_0' (Mev)	B_{max} (gauss) r=8	$A(\rho)$ (kilo-gauss-in.)	ρ (in.)	Ratio B_r/B_{max} r=16.0 in.	r=21.0 in.	r=23.0 in.	r=25.0 in.	r=26.0 in.
30.34	3994	39.86	25.57					
48.64	6403	63.85	25.60	0.919	0.668	0.541	0.422	0.369
50.95	6703	66.91	25.59	0.920	0.669	0.542	0.422	0.371
52.49	6905	68.94	25.58	0.917	0.668	0.540	0.421	0.369
66.23	8762	86.98	25.56	0.917	0.667	0.540	0.420	0.368
76.08	10064	99.92	25.58	0.916	0.666	0.538	0.421	0.367

In addition to making these magnetic-distribution studies, we made another study in which we employed a scattered positron beam created by photons from a 330-Mev synchrotron to determine the necessary correction to our published data. For this determination we used both of these magnetic geometries. That described in Table VI was called the saturation-free geometry. The results of this determination are shown in Fig. 23. They indicate the drastic change in intensity in our spectrometer that was brought about by the causes described in this appendix. On applying these corrections to our published data we find the data to be in good agreement with the results of our new experiment. This agreement is illustrated in Fig. 24. In order

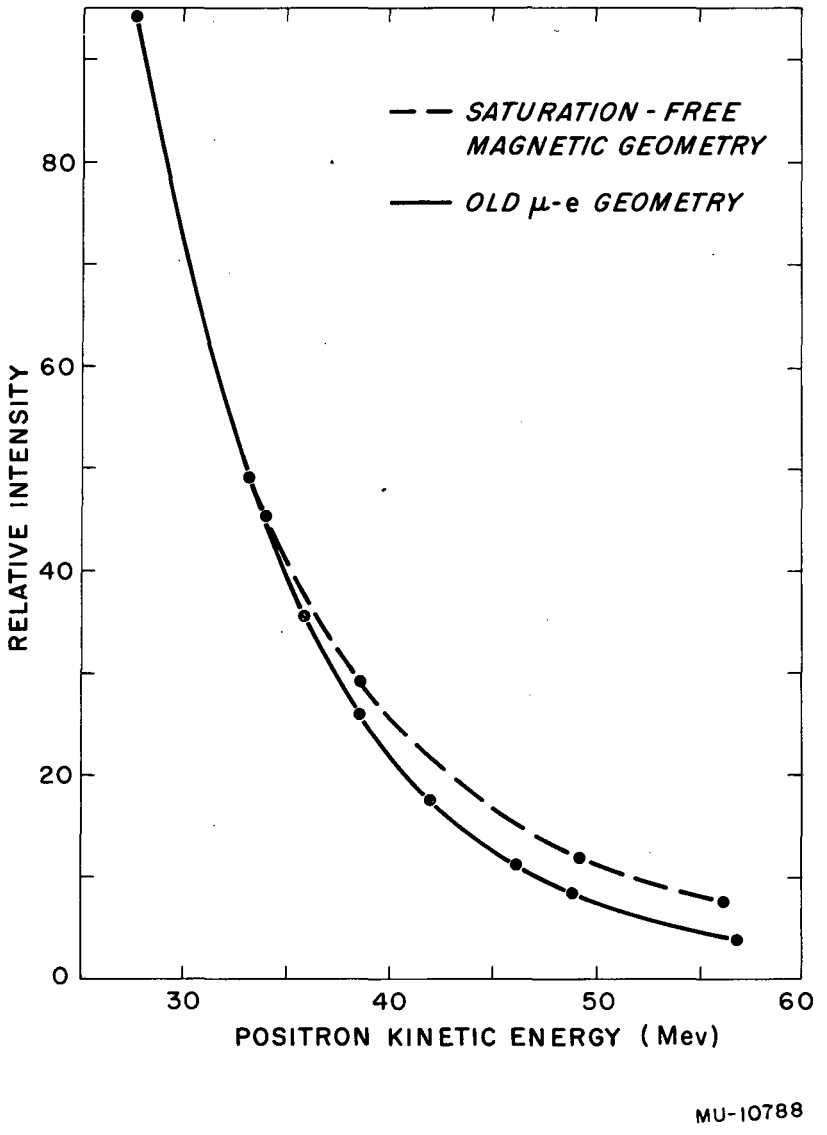

Fig. 23. Experimental results on the effect of increasing magnetic saturation on the measured intensity for a particular spiral-orbit spectrometer geometry.

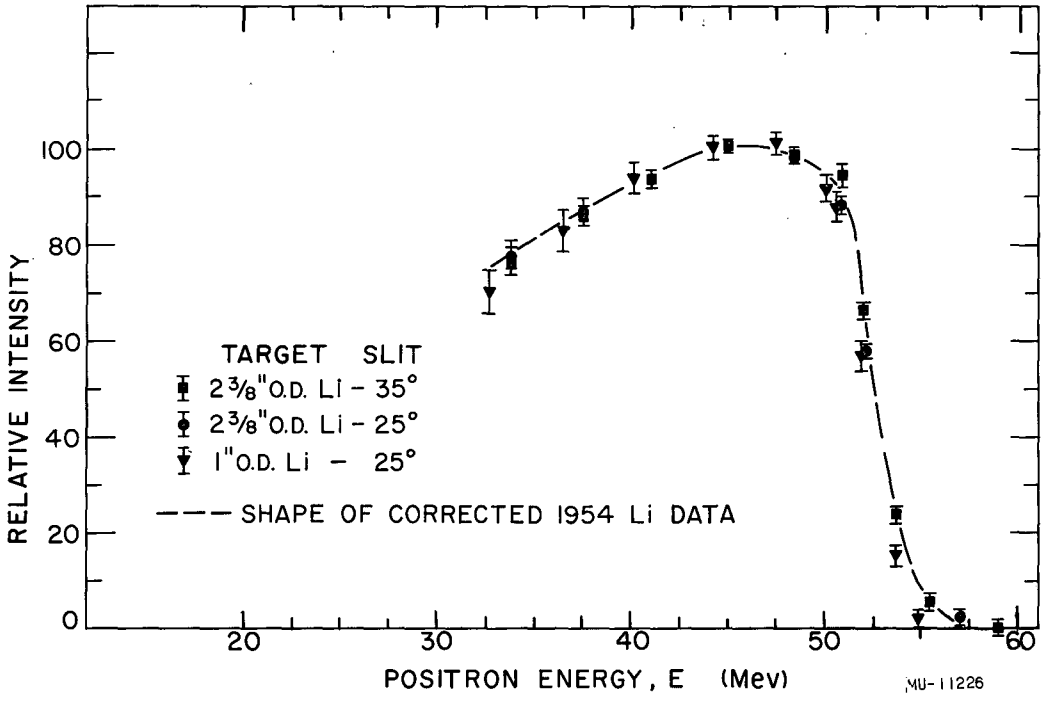

Fig. 24. Comparison of corrected 1954 data with data from this experiment.

to make this comparison on the same figure it was necessary to remove the energy shift that results from positron ionization and radiation losses in the target. For this an average shift was used for each target that was determined from the resolution studies of Appendix A. The different magnetic-resolution effects for each geometry are not removed from these data.

We present this only as an illustration of this agreement and make no further use of our old published data.

C. Radiation Correction

For the function h (η, ΔE) we used the expression for vector and axial vector coupling as derived by Behrends et al.,[8]

$$h_{V,A}(\eta, \Delta E) = \frac{\alpha}{2\pi}\left\{2(U+V) + \frac{6(1-\eta)}{3-2\eta}\ln\eta - 4 + \frac{1}{3\eta}\frac{(1-\eta)}{(3-2\eta)}\left[\left(\frac{5}{\eta} + 17 - 34\eta\right)(\ln\eta + w) + 34\eta - 22\right]\right\}$$

where

$$(U+V) = 2\sum_{m=1}^{\infty}\frac{\eta^m}{m^2} - \frac{\pi^2}{6} - 1 + \ln\eta\left[\ln\left(\frac{1}{\eta} - 1\right) - 2w\right] + \frac{5w}{2} - w^2 + 2(w - \ln 2)(\ln\eta + w - 1) + \left(2\ln\eta + 2w - 1 - \frac{1}{\eta}\right)\ln\left(1 - \eta + \frac{2\Delta E}{m_1 e}\right)$$

Here we have $\alpha = \frac{1}{137}$; $w = \ln(m_1/m_2) = 5.3327$; m_1 = rest mass of the muon; m_2 = rest mass of the electron; $e = 2.71828$; $\eta = E/W$; W = maximum electron energy, and ΔE is the energy interval used in the experiment. To pass from one energy interval ΔE_1 to another interval ΔE_2 one can use the relation

$$h(\eta, \Delta E_2) = h(\eta, \Delta E_1) + \frac{\alpha}{2\pi}\left[2\left(2\ln\eta + 2w - 1 - \frac{1}{\eta}\right)\ln\left\{\frac{(1-\eta)m_1 e + 2\Delta E_2}{(1-\eta)m_1 e + 2\Delta E_1}\right\}\right].$$

Because of a misprint the factor $\alpha/2\pi$ does not appear in the reference cited as the source of this relation. We have calculated the function $h(\eta, \Delta E)$ for different constant ΔE values. Most of the results of our calculations of this function are presented in Table VII. Also appearing in these tables are the evaluated integrals $\Lambda_1(\Delta E)$ and $\Lambda_2(\Delta E)$, where

$$\Lambda_1 = 4\int_0^1 h(\eta, \Delta E)\left[3\eta^2(1-\eta)\right] d\eta.$$

$$\Lambda_2 = 4\int_0^1 h(\eta, \Delta E)\left[\eta^3\right] d\eta.$$

Tables of the function h (η, ΔE) varying by steps of $\Delta\eta = 0.01$ were used throughout all our numerical calculations involving this function.

It should be pointed out that the tabulated values of h (η, $2m_e$) at η=0.10 and η=0.95 disagree with those given by Behrends et al.[8] Our calculation at η=0.95 agrees with Kinoshita and Sirlin,[21] who also point out this fact.

[21] T. Kinoshita, A. Sirlin; Phys. Rev. 107, 593 (1957).

Table VII

Values of $h(\eta, \Delta E)$ as a function of ΔE

η	ΔE (in electron rest-mass units)															
	0	$\frac{1}{4}$	$\frac{1}{2}$	1	2	3	4	5	6	7	8	9	10	12	16	20
.01	4.5619	4.5617	4.5615	4.5611	4.5603	4.5595	4.5586	4.5578	4.5570	4.5562	4.5554	4.55h6	4.5538	4.5522	4.5h90	4.5h59
.03	1.3558	1.3558	1.3557	1.3556	1.3553	1.3551	1.3548	1.3546	1.3543	1.3540	1.3538	1.3535	1.3533	1.3528	1.3518	1.3508
.05	0.66h1	0.66h1	0.66h1	0.66h0	0.6638	0.6637	0.6636	0.663h	0.6633	0.6632	0.6630	0.6629	0.6627	0.6625	0.6619	0.661h
.08	0.3h52	0.3h52	0.3h52	0.3h52	0.3h51	0.3h50	0.3h50	0.3h49	0.3hh8	0.3hh7	0.3hh7	0.3hh6	0.3hh5	0.3hhh	0.3h41	0.3h39
.10	0.256h	0.256h	0.256h	0.256h	0.2563	0.2563	0.2562	0.2562	0.2562	0.2561	0.2561	0.2560	0.2560	0.2559	0.2557	0.2556
.13	0.18h2	0.18h2	0.18h2	0.19h2	0.18h2	0.18h1	0.18h1	0.18h1	0.18h1	0.18h0	0.18h0	0.18h0	0.18h0	0.18h0	0.1839	0.1838
.15	0.155h	0.155h	0.155h	0.155h	0.155h	0.155h	0.155h	0.155h	0.155h	0.155h	0.155h	0.1553	0.1553	0.1553	0.1553	0.1553
.18	0.1267	0.1267	0.1267	0.1267	0.1267	0.1267	0.1267	0.1267	0.1267	0.1267	0.1268	0.1268	0.1268	0.1268	0.1268	0.1268
.20	0.1133	0.1133	0.1133	0.1133	0.113h	0.113h	0.113h	0.113h	0.113h	0.113h	0.113h	0.113h	0.113h	0.1135	0.1135	0.1136
.23	0.098h4	0.098h5	0.098h5	0.098h6	0.098h9	0.09852	0.09854	0.09857	0.09859	0.09862	0.0986h	0.09866	0.09869	0.0987h	0.09883	0.09893
.25	0.09085	0.09086	0.09086	0.09088	0.09091	0.0909h	0.09098	0.09101	0.0910h	0.09107	0.09110	0.09113	0.09116	0.09122	0.0913h	0.091h6
.28	0.08179	0.08180	0.08181	0.08183	0.08187	0.08191	0.08195	0.08199	0.08203	0.08207	0.08211	0.08215	0.08219	0.08226	0.082h2	0.08257
.30	0.07688	0.07689	0.07690	0.07692	0.07697	0.07702	0.07706	0.07711	0.07715	0.07720	0.0772h	0.07728	0.07733	0.077h2	0.07759	0.07776
.33	0.07071	0.07072	0.0707h	0.07076	0.07082	0.07087	0.07093	0.07098	0.07103	0.07108	0.0711h	0.07119	0.0712h	0.0713h	0.07155	0.07175
.35	0.06721	0.06722	0.0672h	0.06727	0.06733	0.06739	0.0674h5	0.06750	0.06756	0.06762	0.06768	0.0677h	0.06779	0.06790	0.06813	0.0683h
.38	0.06264	0.06266	0.06267	0.06271	0.06277	0.0628h	0.06291	0.06297	0.0630h	0.06310	0.06317	0.06323	0.06330	0.063h3	0.06368	0.06392
.40	0.05995	0.05996	0.05998	0.06002	0.06009	0.06016	0.0602h	0.06031	0.06038	0.0604h5	0.06052	0.06059	0.06066	0.06080	0.06107	0.06133
.43	0.05632	0.0563h	0.05636	0.0564h0	0.0564h8	0.05656	0.0566h	0.05672	0.05680	0.05688	0.05696	0.05703	0.05711	0.05726	0.05757	0.05786
.45	0.05h11	0.05h1h	0.05h16	0.05h20	0.05h29	0.05h37	0.05hh6	0.05h5h	0.05h63	0.05h71	0.05h80	0.05h88	0.05h96	0.05513	0.0555	0.05576
.48	0.05106	0.05108	0.05111	0.05115	0.05125	0.05135	0.0514h	0.05154	0.05163	0.05172	0.05181	0.05191	0.05200	0.05218	0.05253	0.05288
.50	0.0h915	0.0h918	0.0h920	0.0h926	0.0h936	0.0h946	0.0h956	0.0h966	0.0h976	0.0h986	0.0h996	0.05006	0.05016	0.05035	0.05072	0.05109
.53	0.0h6h4	0.0h6h7	0.0h650	0.0h656	0.0h667	0.0h678	0.0h690	0.0h701	0.0h712	0.0h722	0.0h733	0.0h7hh	0.0h755	0.0h776	0.0h817	0.0h858
.55	0.0h472	0.0h475	0.0h478	0.0h48h	0.0hh96	0.0h508	0.0h520	0.0h532	0.0h5h3	0.0h555	0.0h566	0.0h578	0.0h589	0.0h612	0.0h656	0.0h698
.58	0.0h220	0.0h22h	0.0h227	0.0h23h	0.0h2h7	0.0h260	0.0h273	0.0h286	0.0h299	0.0h312	0.0h325	0.0h337	0.0h350	0.0h37h	0.0hh23	0.0hh69
.60	0.0h056	0.0h060	0.0h06h	0.0h071	0.0h085	0.0h099	0.0h113	0.0h127	0.0h1h1	0.0h15h	0.0h168	0.0h181	0.0h19h	0.0h221	0.0h272	0.0h322
.63	0.03813	0.03817	0.03821	0.03829	0.038hh	0.03860	0.03876	0.03891	0.03906	0.03921	0.03936	0.03951	0.03965	0.03994	0.0h050	0.0h105
.65	0.03650	0.03655	0.03659	0.03667	0.0368h	0.03701	0.03718	0.0373h	0.03750	0.03766	0.03782	0.03798	0.0381h	0.0384h	0.0390h	0.03962
.68	0.03h0h	0.03h08	0.03h13	0.03h23	0.03h42	0.03h60	0.03h79	0.03h97	0.03515	0.03533	0.03551	0.03568	0.03585	0.03620	0.03686	0.03750
.70	0.03236	0.0324h	0.0326h	0.03256	0.03276	0.03297	0.03316	0.03336	0.03356	0.03375	0.0339h	0.03h13	0.03h31	0.03h68	0.03539	0.03607
.72	0.03063	0.03068	0.03074	0.03085	0.03107	0.03129	0.03150	0.03172	0.03193	0.0321h	0.0323h	0.03254	0.0327h	0.0331h	0.03390	0.03463
.7h	0.02884	0.02890	0.02896	0.02908	0.02932	0.02956	0.02979	0.03002	0.03025	0.0304h	0.03070	0.03092	0.03113	0.03156	0.03238	0.03317
.76	0.02697	0.0270h	0.02710	0.0272h	0.02750	0.02776	0.02801	0.02826	0.02851	0.02876	0.02900	0.0292h	0.0294h7	0.02993	0.03082	0.03167
.78	0.02500	0.02507	0.0251h	0.02529	0.02558	0.02586	0.0261h	0.0264h2	0.02669	0.0269h6	0.02722	0.0274h8	0.0277h	0.0282h	0.02921	0.03013
.80	0.02289	0.02298	0.02306	0.02322	0.02354	0.02386	0.0241h6	0.0244h7	0.0247h	0.02506	0.02536	0.0256h	0.02592	0.0264h7	0.02753	0.02852
.81	0.02178	0.02187	0.02196	0.02213	0.0224h7	0.02280	0.02312	0.0234h5	0.02376	0.0240h7	0.0243h8	0.0246h8	0.02497	0.02555	0.02666	0.02770
.82	0.02062	0.02072	0.02081	0.02099	0.02135	0.02170	0.02205	0.02238	0.02272	0.0230h	0.02337	0.02368	0.02399	0.0246h0	0.02576	0.02685
.83	0.0194h1	0.01951	0.01961	0.01980	0.02018	0.02056	0.02092	0.02128	0.02163	0.02198	0.02232	0.02265	0.02298	0.02362	0.0248h	0.02598
.8h	0.0181h	0.0182h	0.01835	0.01855	0.01896	0.01936	0.01975	0.02013	0.02050	0.02087	0.02123	0.02158	0.02193	0.02260	0.02388	0.02508
.85	0.01680	0.01691	0.01702	0.0172h	0.01767	0.01810	0.01851	0.01892	0.01932	0.01971	0.02009	0.0204h6	0.02083	0.0215h	0.02289	0.02h15
.86	0.01537	0.0154h9	0.01561	0.01585	0.01632	0.01677	0.01721	0.01765	0.01807	0.0184h9	0.01890	0.01929	0.01968	0.0204h	0.02187	0.02320
.87	0.01385	0.01398	0.0141h	0.0143h	0.0148h	0.01536	0.0158h	0.01630	0.01676	0.01720	0.0176h	0.01806	0.0184h	0.01928	0.02080	0.02220
.88	0.01222	0.01236	0.01250	0.01278	0.01333	0.01386	0.0143h	0.0148h	0.01537	0.0158h	0.01631	0.01676	0.01721	0.01807	0.01968	0.02116
.89	0.0104h6	0.01062	0.01077	0.01107	0.01167	0.01225	0.01281	0.01335	0.01388	0.0144h0	0.0149h	0.01539	0.01586	0.01679	0.01850	0.02008
.90	0.00854	0.00871	0.00888	0.00922	0.00987	0.01050	0.01112	0.01171	0.01229	0.01285	0.01339	0.01392	0.0144h	0.0154h	0.01727	0.01895
.91	0.006h2	0.00662	0.00680	0.00718	0.00790	0.00860	0.00928	0.00993	0.01056	0.01118	0.01177	0.0123h	0.01290	0.01398	0.01596	0.01776
.92	0.00h07	0.00h28	0.00h50	0.00h92	0.00573	0.00651	0.00726	0.00799	0.00868	0.00936	0.01001	0.0106h	0.01125	0.012h2	0.01h56	0.01h49
.93	0.001h0	0.00165	0.00189	0.00237	0.00330	0.00h18	0.00503	0.00584	0.00662	0.00737	0.00809	0.00878	0.00946	0.0107h	0.01307	0.01515
.9h	- .00167	-.00138	-.00110	-.0005h	0.00053	0.00155	0.00251	0.003hh	0.00h32	0.00516	0.00597	0.0067h	0.007h9	0.00890	0.011h6	0.01372
.95	-.00531	-.00h96	-.00h62	-.00395	-.00268	-.00h19	-.00036	0.00070	0.00171	0.00268	0.00359	0.00hh7	0.00531	0.00689	0.00971	0.01218
.96	-.00976	-.00933	-.00890	-.00807	-.00652	-.00507	-.00373	-.002h6	-.00128	-.00016	0.00090	0.00190	0.00286	0.00h6h	0.00779	0.01051
.97	-.01551	-.01h93	-.01h36	-.01328	-.01127	-.00945	-.00778	-.0062h	-.00h81	-.003h8	-.00223	-.00105	0.00006	0.00211	0.00567	0.00869
.98	-.02363	-.02276	-.02192	-.02036	-.01755	-.01508	-.01289	-.01092	-.00912	-.007h7	-.0059h	-.00h53	-.00321	-.00080	0.00329	0.00668
.99	-.0375h	-.0358h	-.03h26	-.031hh	-.02677	-.02298	-.01980	-.01705	-.01h6h	-.012h8	-.01053	-.00876	-.00713	-.00h22	0.00058	0.00h45
1.00		-.08629	-.07233	-.05838	-.0hhh2	-.03626	-.030h7	-.02598	-.02230	-.01920	-.01651	-.01hhh	-.01202	-.00835	-.00256	0.00193
$\Lambda_1(\Delta E)$		0.0h108	0.0h170	0.0h238	0.0h317	0.0h372	0.0hh16	0.0hh56	0.0hh91	0.0h52h	0.0h55h	0.0h583	0.0h610	0.0h662	0.0h755	0.0h839
$\Lambda_2(\Delta E)$		0.01534	0.01576	0.01639	0.01739	0.01823	0.01898	0.01967	0.02030	0.02090	0.02146	0.02200	0.02251	0.02346	0.02519	0.02669

UCRL-8202

Correction for last line of Table VII

ΔE (m_e)	$\Lambda_1(\Delta E)$
0	0
$\frac{1}{4}$	0.04453
$\frac{1}{2}$	0.04459
1	0.04471
2	0.04494
3	0.04517
4	0.04538
5	0.04559
6	0.04580
7	0.04600
8	0.04620
9	0.04639
10	0.04658
12	0.04695
16	0.04765
20	0.04831

D. Background Determination

In Fig. 7 we have shown the serious effect of background on the spectrometer-measured value of ρ_M when pions are created in the target that is also used as the source within the spectrometer of positrons from muon decay. Published values on the variation of pion-production cross section with pion energy[3e] illustrate that the desired sources of positrons originate only in a very small pion-energy interval. Pions not in this energy interval leave the production target and imbed themselves in the surrounding areas. Those pions that give rise to muons near or at the surfaces of the spectrometer geometry become an undersirable source of positron background that cannot be distinguished by electronic techniques measuring muon lifetime from positrons that originate in the target. One can screen out some (but not all) of this background. We present the procedures that were used to estimate this background in our experiment, along with other corrections that must be considered in our reduction of the raw data. We present these in the order of increasing influence on the reported data.

1. Correction For Electron Scattering in the Detector

Figure 25 illustrates the experimental procedure that was used to measure the correction for electron scattering in the detector. As shown in this figure, an additional thickness t' of scintillator material was introduced directly in front of the first counter, and quadruple coincidences were measured. The ratio (with its standard deviation) of the number of these coincidences when thickness t' was present to the number when it was absent was determined and is plotted for various thicknesses t' in Fig. 25. These measurements were made at two E_0' energy settings that define the positron-energy interval in which this correction would most seriously affect the measured ρ_M value. We draw the conclusion that within the statistics of these measurements no correction is necessary for positron scattering in our detector.

2. Effect of Muon-Density Distribution

An effect that could seriously change the resolution of the spectrometer and therefore the determined value of ρ_M is the distribution of muons within the target. We tested for this effect in our experiment by changing the size of the incident collimated proton beam (from 1/2 inch in diameter to 3/4 inch in diameter). This was done first for a lithium target 2-3/8-inches in diameter and then for a target 1 inch in diameter. In both cases we found no significant changes in our intensity measurements that would arise from a possible variation of muon density. Table VIII illustrates this with the raw data obtained by use of the 2-3/8-inch target.

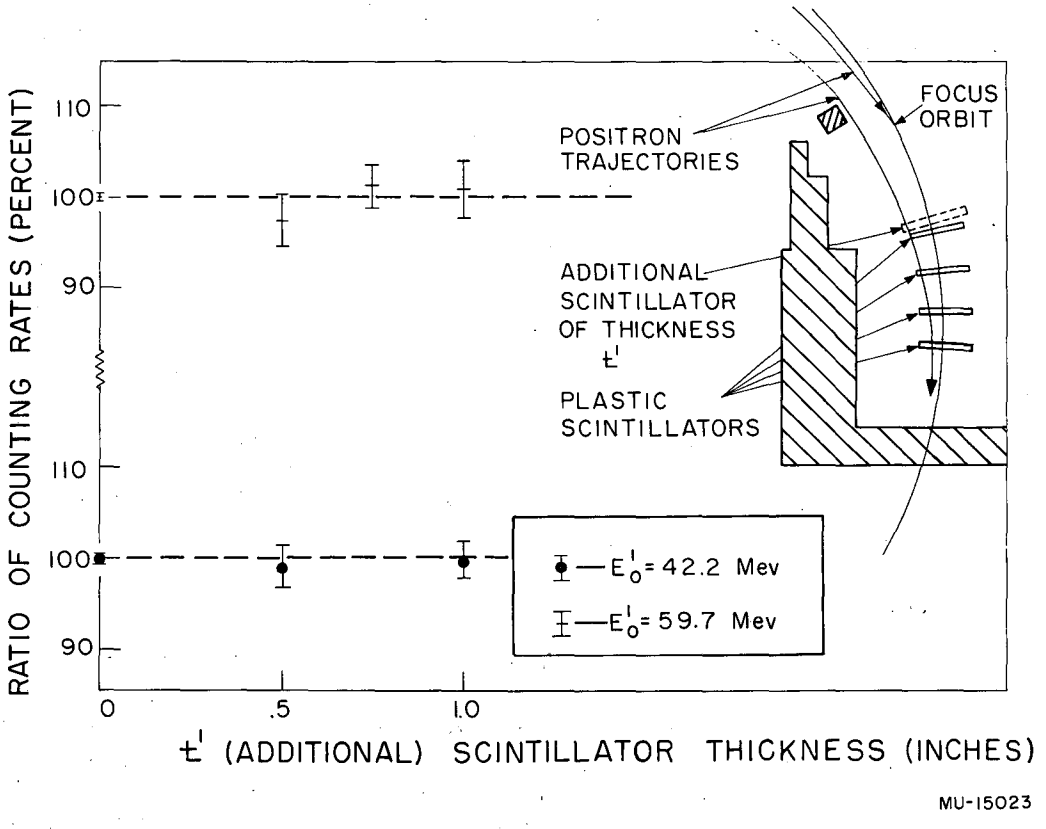

Fig. 25. Results from the experimental study of the correction to the measured intensity for positron scattering in the detector.

Table VIII

Intensity measurements for beams of different sizes (counts minus accidental background divided by magnetic field). (See page 31.)

Diameter of collimated proton beam				
	1/2 inch		3/4 inch	
E'_0	$X(E'_0)$	σ_x	$X(E'_0)$	σ_x
32.9	9.19	0.16	9.17	0.30
46.9	9.85	0.08	9.63	0.26
50.5	6.10	0.11	6.15	0.21

We conclude that within the statistics of these measurements the assumption of a uniform muon-density distribution within the target introduces no serious systematic error in the calculation of our spectrometer resolution functions (Appendix A).

3. Pion "Flyback Effect" Background

In our experiment there are pions that leave the target and remain trapped by the magnetic field in the region between the target and the detector (Fig. 2). Some of these pions, or the muons that arise from their decay, return to the target before the positron is born. The remaining pions decay into muons, which in turn decay into positrons outside the target. We give the name "flyback effect" to the influence of these positrons that originate in the magnetic gap outside the target (but not at the surfaces of the spectrometer geometry) on the measured intensities at the various E'_0 values. We have calculated the effect of this source of positron on the resolution of the spectrometer. We find that its significance becomes apparent only when the proton-beam diameter is larger than the target diameter and at the same time the target diameter is very small. The target and proton-beam conditions that were chosen for the measurement of the ρ_M parameter were such as to render negligible the effect of this positron source. Were this effect significant in our experiment and were it neglected, it would cause us to report too low a ρ_M value.

In addition to our calculations of the influence of the flyback effect on the resolution, we have conducted an experiment that could measure its presence. By reversing the polarity of the magnetic field one brings electrons into focus at the detector position. The sources of these delayed electrons are the negative muons that arise from the decay of the trapped negative pions in this magnetic region. From measurements of negative and positive pion-production cross sections at low pion energies (as shown in Ref. 3e) a ratio of positive to negative pions is determined for the small range of energy for pions that give rise to the muons that decay into positron and electron sources. With this ratio and the electron measurements one

can estimate the contribution to the measured positron intensities of the fly-back effect at each E_0' value. These measurements were made at three E_0' values. Our estimate of the contribution was approximately 0.2%. Calculations yielded values less than 0.1% for the targets that were used.

4. Background Due to Pions Stopping in the Detector

There exists a very small low-energy interval containing pions that satisfy the same focusing conditions as do the desired positrons. The energy of these pions is not sufficient to penetrate through the first scintillator until the energy setting of the spectrometer exceeds the maximum energy of positrons originating in the target. From these pions positrons eventually arise that have a large probability of triggering the electronic system. If one neglected the effect of this positron source and if it were significant, it would result in an overestimate of the ρ_M parameter.

We have measured the magnitude of this positron source, at three E_0' values, by the following procedure. First the spectrometer resolution was determined for pions that would reach the detector at the chosen E_0' positron-energy setting. This resolution function was used to decide on the thickness of a CH_2 pion-energy degrader that should be used at this E_0' setting to degrade the energy of these pions sufficiently that they would be deflected by the magnetic field and miss the first counter. As shown in Fig. 2, intensity measurements were made with absorber in and absorber out. Our measurements showed the positron intensity for absorber in 1% less than the intensity with absorber out at positron energy settings of E_0' = 33 and 48 Mev. No change in the intensities was observed at E_0' = 58 Mev, at which positron setting the pions have sufficient energy to pass through the first counter. These measurements were accurate to 2%. We give significance to these measurements because at the two positron energy settings (E_0' = 33 and 48 Mev) both positron-intensity measurements with CH_2 absorber in were low. In the reduction of our raw data a constant 1% background was attributed to this effect over the measured range of positron energies below E_0' - 58 Mev. Because this effect was small in our experiment, we ignored the slow increase of this background with increasing E_0' settings for positrons. The increase of this background results from the increase in the pion-production cross section in this pion energy region.

5. Background from Pions Stopping in Pole-Tips

The largest contribution to the background arises from pions stopping in the pole tips of the spectrometer. Equations expressing the focusing properties of the spectrometer show that the probability of particle detection increases with a decrease of the radius r_0 of the particle source, which is measured from the axis of magnetic symmetry. The contribution of this background to the measured positron intensities can be determined experimentally. Our procedure for measuring this contribution is illustrated in Fig. 26. In addition to this illustration, Figs. 1 and 2 are an aid to an understanding of the experimental procedure.

Shown in Fig. 26 is the configuration of the source that is used in these measurements. The original lithium target is positioned inside a thick-walled hollow cylindrical shield made of lead. This assembly is mounted on one side of the median plane of the spectrometer. The wall of the lead cylinder is 2.5 inches thick. This thickness is sufficient to stop all

(a) positrons originating in the target that would be focused into the detector,

(b) pions that are created in the target and are emitted into space on the source side of the median plane (except those passing out from the magnet),

(c) positrons eventually arising from pions that stop in the lead shield.

Pions emitted by the target into space opposite to the source side of the median plane embed themselves in the pole of the spectrometer. Some of the positrons that eventually arise because of the presence of these pions at the pole are focused into the detector.

We were able to make significant measurements of the contribution of this background to the measured intensity because of the large counting rates that are obtained in using a spiral-orbit spectrometer. Measurements of this contribution as obtained by this method for one spectrometer geometry ($\Theta' = 35^{\circ}$; 2-3/8-inch-diameter lithium target) are shown in Fig. 26. The best polynominal that represents this set of data was obtained by least-squares fitting and the minimum-χ^2 methods. We treated the result that arose from this polynominal expression as one-half the contribution of this background to the measured intensity at the desired E_0' value that was reported as raw data. As seen, the effect of this background on the raw data is very significant in our experiment. Were this background contribution ignored the reported ρ_M value (as shown in Fig. 7) would have been between 0.68 and 0.70.

6. Background from Pions Stopping in the Counter Shield

The most uncertain background in our experiment results from pions stopping in the lead shield that screens the counters from the secondary particles that are produced during target bombardment by a proton pulse (Figs. 2 and 27). In one of our unreported experiments we tried to eliminate this lead shield. Our true counting rates were thereupon seriously impaired by the necessary increase in the delay time between the proton pulse and the first gate during which counts were collected. In addition, the background contribution to the measured intensities from pions stopping in the magnetic poles also increased. Because of these serious disadvantages we chose to use this lead shield in our experiments.

It is not practical to directly measure the contribution of this background to the raw data. In our study of this background effect we first determined the resolution for the system shown in Fig. 27 when placed in the nonuniform magnetic field as illustrated by Fig. 4. We assumed a uniform positron-source distribution over the faces of the lead shield exposed to positive pions. Then, by folding this resolution into a modified Michel distribution (Eq. (4)), we determined a curve representing the behavior of the intensity of this background with positron-energy setting E_0'. In this

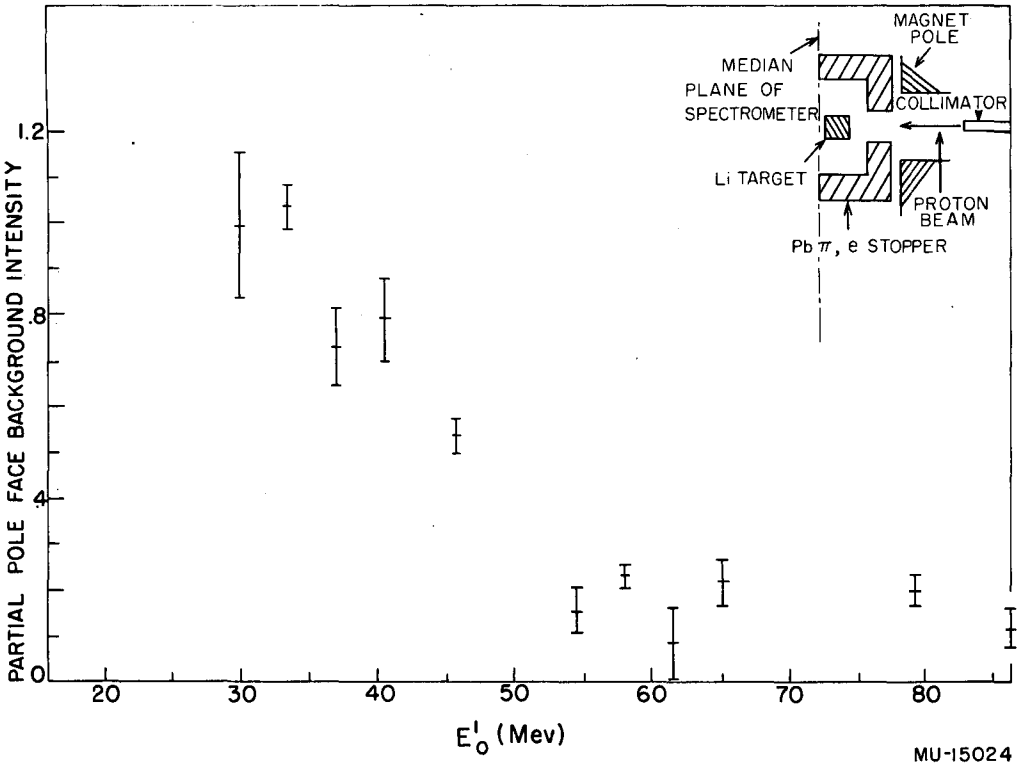

Fig. 26. Measured background from pions stopping in spectrometer pole faces as a function of positron energy at the focus orbit.

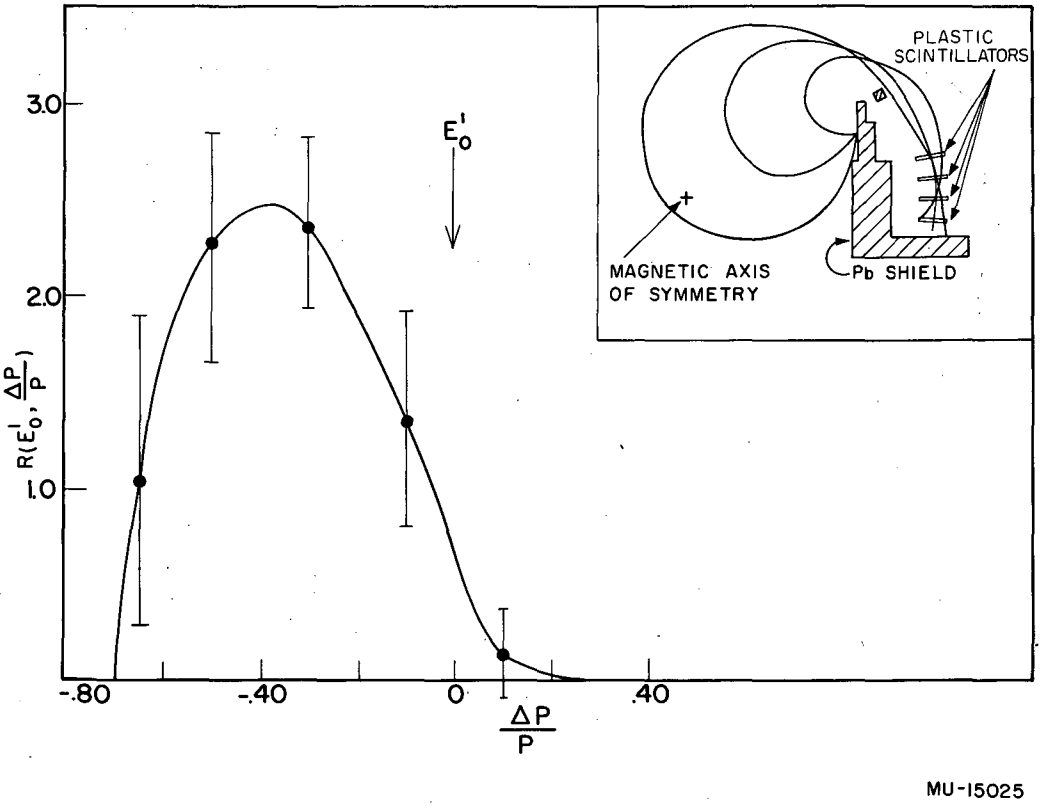

Fig. 27. Magnetic resolution for a broad positron source resulting from pions stopping in the lead detector shield.

study we used the Michel parameter $\rho_M = 0.70$. The intensity distribution that arises from these calculations is very flat, so that no significant difference in shape results if the parameter ρ_M is changed by ± 0.05. In these studies we employed

(a) a mechanical orbit plotter that traces out trajectories of a charged particle having a given momentum as it moves in a particular magnetic field distribution,

(b) an IBM 650 computer.

In our study of the resolution of the broad positron source as shown in Fig. 27 we considered not only the simple trajectories that are shown in this figure, but also the more complex trochoidal trajectories that might arise. The probability of detecting charged particles having these more complex trajectories is very small. This would not be true if a positron source could arise at the base of the lead shield. Since only negative pions can reach this base, no delayed-positron source can be emitted from this surface. Shown also in Fig. 27 is the resolution for this geometry that arises from our calculations. The quoted errors indicate our estimate of the accuracy to which these calculations were carried.

To determine the magnitude of this background we made measurements, during the regular experiment, of total background beyond the E_0' energy cut-off of the desired spectrum, as shown in Fig. 7. From this measured total background in the positron-energy region of $E_0' > 57.5$ Mev we subtracted the contribution of the background as is obtained for pions stopping in the poles of the magnet (Part 5 of this Appendix). The remaining background was considered to be from the lead shield. This residual background in the positron energy region of $E_0' \geq 57.5$ Mev was used to obtain the desired normalization for the above calculated positron-intensity distribution as a function of E_0' that was obtained for a positron source from this lead shield. From this normalized distribution curve the contributions to the measured intensities of the background that results from pions stopping in the lead shield were determined in the positron energy region of $E_0' < 57.5$ Mev.

E. Time-Scale Calibration for Determination of Muon Mean Lifetime

The determination of the muon mean lifetime depends on knowing the time widths of the gates and the dead times between them; which establish that particular moment - which we call the instant of the mean counting rate - at which we could represent by an instantaneous counting rate all the counts occurring within the duration of any one gate. (Because of the finite lifetime of the particles, this time of the mean counting rate occurs before the midpoint of the gate duration.) We define the time from "zero" up to this moment as the sum of

(a) the delay, after the proton pulse, of the start of the first gate,

(b) the total of the time widths and dead times between the gates of all the foregoing gates, and

(c) the time from the start of the gate in question until the instant of the mean counting rate.

The absolute measure of time (a) is not important for a lifetime measurement. Its setting is governed by the magnitude of the accidental counting rate. We have measured Interval (b) by photographing the active time of each gate and the dead time between gates on a calibrated time scale. For a measure of the gate width the sine wave of a 10-megacycle Tektronix time-mark generator (accuracy 50 cycles per megacycle) was fed into the amplifier section of a Tektronix 517 oscilloscope. The amplified signals were then used as input into the tandem gate unit. A Berkeley Instruments double-pulse generator triggered the tandem gate and also the sweep circuit of another 517 Tektronix oscilloscope on which the output from each gate was displayed. The display of each individual gate width was photographed together with the superimposed sine wave. Approximately twenty such oscilloscope displays were photographed for each gate. Under magnification we could see that the error of measuring the number of sine waves displayed during the active time of the gate was less than one-half cycle. For each gate the active time was defined as the time between the half height of the voltage ordinate during the start of the gate and that at the cutoff. In our reduction of the data we used the time width of each gate and its error as obtained from the arithmetic mean of these measurements. Each gate width was approximately two microseconds. The gate widths of the four gates were the same within 5%.

The dead time between adjacent gates was measured in the same manner except for small modifications. In this measurement the sine wave of a 50-megacycle Tektronix time-mark generator was used. The signal from this source was fed directly to the oscilloscope. Superimposed on the same photograph were the rise and cutoff portions of the two adjacent gates. The number of sine waves displayed during the nonactive time between gates was measured under magnification. The arithmetic mean of such measurements was used as the dead time between gates.

Interval (c) is obtained by a calculation relating the counting rate for the measured gate width to the instantaneous counting rate corresponding to the decay rate for particles having the mean life in question. For exactly equal gate time widths no error is introduced in calculating the time of Interval(c) by the assumed value of the mean lifetime, because a measurement of the lifetime is independent of the origin of the time scale. An error of 10% in the assumed mean lifetime introduces a shift of approximately 1% in the time given by Interval (c) for our system. Because the gate time widths in our system are approximately equal, a 10% variation of the assumed mean life introduces a maximum error of 0.001 microsecond in the time used for a particular gate. These errors, corresponding to errors in the time of the mean counting rate of a gate, do not influence the data appearing in Table II.

In the treatment of our data we simplified our calculations of the mean lifetime by considering that there was no error in the time of the mean counting rate. This simplification introduces a maximum additional error of 0.005 μsec in the mean lifetime. This error is in addition to that obtained from a statistical treatment of the data in which errors from the time widths of gates and the number of counts are taken into account. We have allowed for this additional error in reporting the accuracy of the weighted mean value of the mean lifetime as given in Table II.

Information Division
br